Evidence supporting an antimicrobial origin of targeting peptides to endosymbiotic organelles

Clotilde Garrido[1]†, Oliver D. Caspari[1]†, Yves Choquet[1], Francis-André Wollman[1], Ingrid Lafontaine[1*]

Affiliations:

[1]UMR7141, Institut de Biologie Physico-Chimique (CNRS/Sorbonne Université), 13 Rue Pierre et Marie Curie, 75005 Paris, France.

† These authors contributed equally to this work

* Corresponding author

Email: ingrid.lafontaine@ibpc.fr

Keywords: Chlamydomonas, targeting peptides, antimicrobial peptides, primary endosymbiosis, import into organelles, chloroplast, mitochondrion.

Short tittle: Antimicrobial origin of organelle targeting peptides

Author Contributions

Conceptualisation: FAW, IL; Data Curation: CG, ODC, IL; Funding Acquisition: YC, FAW, IL; Investigation and Validation: CG and IL (computational), ODC (experimental); Software: CG, ODC; Supervision: YC, FAW, IL; All authors contributed to writing and editing the manuscript.

This file contains:

- Main manuscript
- Figure legends 1-7
- Figures 1-7

Abstract

Mitochondria and chloroplasts emerged from primary endosymbiosis. Most proteins of the endosymbiont were subsequently expressed in the nucleo-cytosol of the host and organelle-targeted via the acquisition of N-terminal presequences, whose evolutionary origin remains enigmatic. Using a quantitative assessment of their physico-chemical properties, we show that organelle targeting peptides, which are distinct from signal peptides targeting other subcellular compartments, group with a subset of antimicrobial peptides. We demonstrate that extant antimicrobial peptides target a fluorescent reporter to either the mitochondria or the chloroplast in the green alga *Chlamydomonas reinhardtii* and, conversely, that extant targeting peptides still display antimicrobial activity. Thus, we provide strong computational and functional evidence for an evolutionary link between organelle-targeting and antimicrobial peptides. Our results support the view that resistance of bacterial progenitors of organelles to the attack of host antimicrobial peptides has been instrumental in eukaryogenesis and in emergence of photosynthetic eukaryotes.

41 ## Introduction

42 Mitochondria and chloroplasts are eukaryotic organelles that evolved from bacterial
43 ancestors through endosymbiosis (see [1] and [2] for recent reviews). These endosymbiotic events
44 were accompanied by a massive transfer of genetic material from the bacterial ancestors to the host
45 genome through what is known as Endosymbiotic Gene Transfer (EGT; [3]). Thus, to be
46 successful, primary endosymbiosis required the establishment of efficient protein import
47 machineries in the envelope membranes of the proto-organelle to re-import the products of the
48 genes transferred to the nuclear genome. As a result, most mitochondrial and chloroplast genomes
49 encode less than 100 proteins and the majority of proteins localised therein (ca. 1000 in
50 mitochondria and >2000 in the chloroplast) are now translated in the cytosol and imported into the
51 organelle [4,5]. Most nuclear-encoded proteins found in organelles harbour a targeting peptide
52 (TP), an N-terminal presequence functioning as an address tag, *i.e.* determining the subcellular
53 localisation of cargo proteins within endosymbiotic organelles [6]. TPs are recognised by the main
54 mitochondrial and chloroplast translocation pathways [7,8] and destroyed upon import into
55 organelles [4,5]. The emergence of TP-based import, despite being a key innovation enabling
56 endosymbiosis and eukaryotism, remains poorly understood [8–10].

57 As described in a proposed scenario summarised in Supplementary Figure 1 for the
58 emergence of the endosymbiotic protein import system [11], TPs may originate from antimicrobial
59 peptides (AMPs). Archaea, bacteria and eukaryotes alike use antimicrobial peptides (AMPs) as
60 part of their innate immune system to kill microbes, typically via membrane permeabilisation
61 [12,13]. Numerous studies have established that AMPs consistently play a role in most symbiotic
62 interactions [14,15], which argues for their involvement in the initial relationship between a host
63 and a proto-endosymbiont. Extant heterotrophic protists employ AMPs to kill engulfed prey, which
64 suggests that early eukaryotes likely used AMPs in a similar way against their cyanobacterial prey
65 that ultimately became the chloroplast [16]. Similarly, the archaeal host will have delivered AMPs
66 against the α-proteobacterial ancestor of mitochondria, whether it was a prey or an intracellular
67 pathogen akin to Rickettsiales [17,18]. AMPs might also have been instrumental when considering
68 mutualism at the origin of endosymbiosis, since present-day hosts use non-lethal concentrations of
69 AMPs to control the growth of symbionts and to facilitate metabolic integration by enabling
70 nutrient exchange [12,19].

71 Studies of the various extant strategies for microbial defence against AMPs have revealed
72 instances where AMPs are imported into bacterial cells via dedicated transporters and then
73 degraded by cytoplasmic peptidases, hereafter referred to as an "import-and-destroy" mechanism
74 [20–26], which is strikingly reminiscent of TP-based import.
75 EGT thus would have started with incorporation of DNA fragments from lysed bacteria into
76 the host genome, as observed in extant phagotrophic protists [27,28]. Endosymbiotic integration
77 was then promoted through acquisition, by the proto-endosymbiotic bacteria, of an import-and-
78 destroy mechanism to resist the AMP attack from the host. The serendipitous insertion of a bacterial
79 gene downstream of an AMP coding sequence in the host genome, whether right upon EGT or after
80 chromosomal rearrangements, then allowed the import of its gene product back into the proto-
81 organelle via the very same inner membrane transporter that allowed the AMP-resistant
82 endosymbiont to detoxify attacking peptides.
83 Indeed, extant TPs continue to show structural similarities to a type of AMP called Helical
84 Amphiphilic Ribosomally-synthesised AMPs (HA-RAMPs), which are characterised by the
85 presence of a cationic, amphiphilic α-helix [11,29,30] . Mitochondrial TPs (mTPs) contain a similar
86 positively charged helix, the amphiphilic character of which is crucial for import [31–33]. The
87 secondary structure of chloroplast TPs (cTPs) has been a matter of debate. They are longer than
88 mTPs and contain parts that are not helical, such as an uncharged N-terminus thought to play a role
89 in defining organelle specificity [6,34–36]. Most cTPs appear unstructured in aqueous solution
90 [37], yet NMR studies using membrane-mimetic environments have demonstrated that cTPs also
91 contain positively charged, amphiphilic α-helical stretches [38–40], suggesting cTPs fold upon
92 contact with the chloroplast membrane [41].
93 Here, we tested the hypothesis that TPs have originated from host-delivered AMPs. If
94 their common origin holds true, enduring similarities in their physico-chemical properties should
95 have remain despite their large evolutionary distance. In addition, at least a subset of TPs and HA-
96 RAMPs may still display some dual antimicrobial and organelle targeting activities. Here, we used
97 the unicellular green alga *Chlamydomonas reinhardtii* to show that these two predictions are
98 fulfilled, thus providing solid evidence that bacterial resistance to the host stands at the core of the
99 emergence of eukaryotism.
100

We first assess in depth the physico-chemical properties of the various families of HA-RAMPs using a consistent set of descriptors and propose a more robust classification of these peptides compared to the current AMP families. We next provide computational evidence for the extensive overlap of the physico-chemical properties of TPs with those of a cluster of HA-RAMPs. Finally, we demonstrate experimentally that extant antimicrobial peptides are able to target a fluorescent reporter to either the mitochondria or the chloroplast of the *C. reinhardtii* and show that targeting peptides still display antimicrobial activity.

Methods and Materials

Sequence Data Set

The groups of peptides used in this study and the corresponding data sources are given in Table S1. Detailed information for each targeting, signaling, antimicrobial and random peptides are given in Tables S2 to S5. Antimicrobial peptides were extracted from the CAMP$_{R3}$ database [42]. We selected the families of antimicrobial peptides based on the following criterion: i) activity experimentally validated, ii) documented amphiphilic α-helical structure, with at least one family member with a resolved 3D structure available in the Protein Data Bank [43], iii) documented activity of bacterial membrane destabilisation. For 3 families comprising peptides with very different structures, additional filtering was applied. We recovered only the bacteriocin of type IIa that are characterised by an amphiphilic helix [44] in BACTIBASE [45]. We selected only those defensins with a resolved 3D structure with at least 5 consecutive residues in a α-helix and only those cathelicidins with a resolved structure or defined as an amphiphilic helical peptide in [46] via UNIPROT. As a negative control, we retrieved the cyclotides of globular structure. TPs with experimentally-confirmed cleavage sites were recovered from proteomic studies (see Table S1). 200 eSPs were randomly extracted among 4707 confirmed eSPs from the Signal Peptide Website (http://www.signalpeptide.de). eSPs were selected so as to follow the length distributions of the peptides from HA-RAMP class I families. 200 random peptides were generated following the amino-acid frequencies observed in the Uniprot database and the length distribution of TPs. Data sets were curated to exclude sequences shorter than 12 amino acids or longer than 100 amino acids, following the length distributions of the peptides from HA-RAMP class I families.

Peptide description and Auto-Cross Covariance (ACC) Terms

As amino acid descriptors, we used the Z-scales established by Hellberg and colleagues [47]. ACC terms between Z-scales were computed as described previously in [48]. ACC terms combine auto-covariance (same z-scale i = j) and cross-covariance (different z-scale i ≠ j) of neighboring amino acids over a window of 4 residues (lags (l) ranging from 1 to 4). There are thus nine nearest neighbor ACC terms for the 3 z-scales factors, yielding 36 ACC terms per peptide of length N. Each ACC term is defined for a given Z-scale couple (i,j) as follows:

$$ACC_{i,j,l} = \sum_{n=1}^{N} -l \frac{z_{i,n} \times z_{j,n+l}}{N - l}$$

The Z-scales values were retrieved from the AAindex database (https://www.genome.jp/aaindex/) via the R package protr (v1.5-0). ACC terms were calculated with the acc function from the same R package and pre-processed by mean-centering and scaling to unit variance.

To assign a hydrophobicity value to a given peptide, we select the highest value obtained for a sliding window of 9 residues along the peptide. We used the hydrophobicity indices of amino acids estimated by octanol/water partitioning [49] to determine the mean hydrophobicity of the 9-residues window. The net charge of a peptide is the sum of the positively charged residues (arginine and lysine) and of the negatively charged residues (glutamate and aspartate) at pH 7.4.

The number of residues along the peptide that can theoretically adopt an amphiphilic helical structure is calculated as follows: The peptide is drawn along an α helical wheel and the longest region (of at least 9 residues) of the peptide that can adopt an amphiphilic helix is searched following the same criterion as in Heliquest [50]. The helix net charge corresponds to the net charge of these predicted amphiphilic helix.

K-means clustering

Peptides were clustered based on the Euclidean distance defined above by k-means (scikit-learn Python package version 0.21.2). Centroid initialisation was performed with the 'k-means++' method with the best inertia among 100 runs for k ranging from 2 to 10. The selected k value (2) is that leading to the best average silhouettes coefficient -a measure of the clustering quality- [51] over all peptides.

160 ## Distance trees

161 Euclidean distances between pairs of 36-dimensional vectors defining each peptide with their
162 ACC terms were used to compute a distance tree between the studied HA-RAMPs, with the
163 neighbor-joining implementation of the scikit-bio Python library, version 0.5.5. To evaluate the
164 robustness of bipartitions on that NJ tree, we built 1000 trees from bootstrap ACC vectors and
165 determined internode certainty (IC) and tree certainty (TC) measures [52] implemented in RaxML
166 v8.2.12 [53]. Tree annotation and display was performed with iTOL v5.5 [54].
167

168 ## Vizualisation of peptide properties

169 The two (or three) principal components of a Principal Component Analysis (PCA) of the peptides
170 defined by their 36 ACC terms were used for visualisation of the peptide's properties. The weights
171 of each variable in the PCA are summarised by correlation circles in Supplementary Figure 5.
172 Analyses were performed with the scikit-learn Python package version 0.21.2. Box plots were
173 generated with the R ggplot2 package version 3.1.0.
174

175 ## Detection of cTP motifs in HA-RAMPs

176 Scripts for finding Hsp70 binding sites and FGLK motifs were developed in R, exactly
177 following the rules described by [55] and [56], respectively.
178

179 ## Strains and culture conditions

180 *C. reinhardtii* cells derived from wild-type strain T222+ (*nit1*, *nit2*, *mt+*) were grown in
181 mixotrophic conditions in Tris-acetate-phosphate (TAP) medium [57] under ~30 µmol photons m^{-}
182 ^{2} s^{-1} at 25°C, either in 200 µL in 96-well plates for 3-4 days or in agitated Erlenmeyer flasks of 200
183 mL. Constructs were transformed into strain T222+ by electroporation and transformants, selected
184 for paromomycin resistance, were screened for high Venus expression in a fluorescence plate
185 reader (CLARIOstar, BMG labtech) as described in [58].
186

187 ## Generation of constructs

188 Constructs were made by inserting sequences coding for candidate peptides directly upstream
189 of the Venus start codon in plasmid pMO611, kindly provided by the Pringle lab. pMO611 is a

190 derivative of the published bicistronic expression plasmid pMO449 [58] in which translation of the
191 eight first RBCS codons ahead of the Venus coding sequence was prevented by mutating the start
192 codon to CTG. To increase expression of the AMP constructs, we modified plasmid pMO611
193 further by inserting RBCS2 intron 2 within Venus, 73 bases downstream of the initiation codon.
194 Introns do not influence targeting. Native Chlamydomonas TP sequences were amplified from
195 strain T222+ genomic DNA, while codon optimised AMP gene sequences were synthesised by
196 Eurofins Genomics. Sequences used are detailed in Table S6. Peptide constructs were assembled
197 and integrated upstream of Venus using the NEBuilder HiFi Assembly kit (New England Biolabs).
198 Correct assembly was verified by sequencing of inserts and flanking regions. Linear transformation
199 cassettes were excised from plasmids with *Eco*RV (New England Biolabs) prior to transformation.
200

201 ## Microscopy

202 For confocal imaging (Figure 5 and Supplementary Figures 9), cells were subjected to 0.1
203 μM MitoTracker Red CMXRos (ThermoFisher) for 30 minutes in the dark and washed with TAP
204 prior to imaging on an upright SP5 confocal microscope (Leica). Venus (excitation 514 nm/532-
205 555 nm emission) and MitoTracker (561 nm/573-637 nm) were imaged sequentially to avoid
206 crosstalk, each alongside chlorophyll autofluorescence (670-750nm emission) to eliminate cells
207 that had moved between images (chlorophyll data from 514 nm excitation shown in figures).
208 Epifluorescence images (Supplementary Figures 7 and 10) were taken on an Axio Observer.Z1
209 inverted microscope (Zeiss) equipped with an ORCA-flash4.0 digital camera (Hamamatsu) and a
210 Colibri.2 LED system (Zeiss) for excitation at 505 nm for Venus (filter 46HE YFP shift free, 520-
211 550nm emission) and 470 nm for chlorophyll autofluorescence (filter set 50, 665-715nm emission)
212 with cells in poly-L-lysine (Sigma Aldrich) coated 8-well μ-slides (Ibidi). Image brightness was
213 adjusted for presentation in figures and cyan, yellow and magenta linear lookup tables, assigned to
214 MitoTracker, Venus and chlorophyll channels respectively, in Fiji (http://fiji.sc/Fiji, version 2.0.0-
215 rc-69/1.52p). To quantify co-localisation (Supplementary Figure 9), cells were cropped out of
216 larger fields-of-view using a standard region-of-interest quadratic box with 13 μm side length in
217 Fiji. Fiji was also used to measure image background intensities from outside the cell for the Venus
218 channel, or from within the cell but outside the organelle in the case of the MitoTracker and
219 chlorophyll channels. Backgrounds were then substracted and Pearson correlation coefficients
220 were calculated as a measure of co-localisation [59].

221

222 ## Biochemistry

223 Chloroplasts and mitochondria were isolated essentially as described in [60], with the
224 following modifications. Protease assay data (Figure 6C,D) and purity data (Figure 6A,B) came
225 from two different extractions (a) and (b) respectively, which were done as follows. 2 L cultures
226 inoculated either into TAP 48h before the experiment and grown at 50 µE m^{-2} s^{-1} (a), or in Minimal
227 Medium 72h before the experiment and grown aerated under at 200 µE m^{-2} s^{-1} (b), were kept in
228 darkness the night preceding the experiment. Cells were washed twice in 20 mM HEPES-KOH pH
229 7.2 (a), or washed once in 10 mM HEPES-KOH pH 7.2 and then subjected to an acid shock to
230 remove flagella as described in Craige et al. (2013) (1min at pH 4.5 by adding 1M acetic acid, then
231 neutralising back to pH 7.2 with 1M KOH) (b). Working in a cold room, cells were then
232 resuspended in 50 mL ice cold breaking buffer (300 mM Sorbitol, 3 mM $MgCl_2$, 5 mM EDTA,
233 0.5% Polyvinylpyrrolidone PVP40, in 67 mM HEPES-KOH pH 7.2) and disrupted by nebulisation
234 with Argon using either one pass at 40 psi (a), or four passes at 80 psi (b), after which an aliquot
235 was set aside. A brief centrifugation up to 4000 g (8 °C, manual stop when reaching 6000 RPM,
236 Beckman JA-12) was used to separate chloroplast and mitochondrial fractions in pellet and
237 supernatant respectively. Chloroplasts were recovered at either the 45/70% (a) or the 20/40% (b)
238 interphase of a 12 ml discontinuous Percoll gradient (in chloroplast wash buffer: 300 mM Sorbitol,
239 3 mM MgCl2, in 67 mM HEPES-KOH pH 7.2) after 2 h of ultracentrifugation (4 °C, 5000 RPM,
240 Beckman SW41, slow acceleration and deceleration) and washed in 5 volumes of chloroplast wash
241 buffer (8 °C, manual stop when reaching 3000 RPM, Beckman JA-20, acceleration: 5, deceleration:
242 0). Mitochondria were purified using a series of differential centrifugations: 20 min at 1500 g to
243 pellet residual chloroplasts (8 °C, 3500 RPM, Beckman JA-12), 20 min at 20 000 g to pellet
244 mitochondria (8 °C, 11 300 RPM, Beckman JA-13.1), 40 min at 20 000 g (8 °C, 11 300 RPM,
245 Beckman JA-13.1) to run a 30 ml 20% Percoll purification (in 250 mM Sorbitol, 1 mM EDTA,
246 0.5% PVP40, in 10 mM MOPS-KOH pH 7.2) of which the bottom ~3 mL were kept, and further
247 centrifuged 20 min at 20 000 g (8 °C, 11 300 RPM, Beckman JA-13.1) to pellet mitochondria after
248 Percoll removal by dilution with 40 mL mitochondrial wash buffer (250 mM Sorbitol, 1mM EDTA,
249 in 10 mM phosphate buffer pH 7.2). Isolated organelle pellets were resuspended in 100 µL SEM
250 (250 mM Sucrose, 1 mM EDTA, in 10 mM MOPS-KOH pH 7.2). For the proteinase assay [60], a
251 22 µL aliquot of isolated organelles was treated with 1.1 µL 25 % Triton X-100 for 5 min on ice,

252 another with an equal volume of water. Each sample was split into two aliquots of 10.5 µL, one of
253 which was treated with 0.5 µL proteinase K 20x stock in SEM (final concentration: 150 µg/mL)
254 for 15 min on ice, and the other with an equal volume of SEM. All aliquots were then treated with
255 0.25 µL 100 mM PMSF and 2.8 µL 5x storage buffer (5x Roche cOmplete^{TM} Mini proteinase
256 inhibitor cocktail, 50 mM NaF, 1 M DTT, 1 M Na_2CO_3) and stored at -20°C. Of each isolated
257 organelle and whole cell sample, an aliquot was precipitated overnight at 4°C by adding 900 µL
258 80% Acetone, pelleted for 10min (4°C, max speed, Eppendorf 5415 D benchtop centrifuge), dried
259 for ~10min under vacuum, resuspended in protein resuspension buffer (2% SDS, 10 mM NaF, 1x
260 Roche cOmplete Mini proteinase inhibitor cocktail, in 100 mM Na_2CO_3) and used for protein
261 quantification by BCA assay (ThermoFisher Scientific). Samples were then run on either 4-15%
262 (a) or 8-16% (b) precast gels (Biorad), transferred onto 0.1µm nitrocellulose membranes and used
263 for immunoblot detection. To be able to probe a very limited amount of sample with multiple
264 antibodies, membranes were cut horizontally into separately treated strips. Primary antibodies
265 raised against the following proteins were used in block buffer (5% BSA, 0.1% Tween-20, in PBS)
266 at the indicated dilutions: α-Tubulin (Sigma Aldrich T5168, 1:50,000), FLAG (Agrisera AS15
267 2871, 1:10,000), COXIIb (Agrisera AS06 151, 1:10,000), BIP (Agrisera AS09 481, 1:2000), CF1β
268 (homemade, rabbit, 1:50,000) [62], OEE2 (homemade, rabbit, 1:2000) [63], RBCS (kindly
269 supplied by Spencer Whitney, rabbit, 1:20,000) [64], NAB1 (Agrisera AS08 333, 1:10,000). ECL
270 signals were recorded on a ChemiDoc Touch (Biorad). Blots were cropped and final figures
271 assembled in Powerpoint.
272

273 Antimicrobial activity assays

274 Standard minimum inhibitory concentration broth microdilution assays in the presence of
275 BSA/acetic acid were performed in triplicate as described in [65] using peptides chemically
276 synthesised to ≥95% purity (Proteogenix). Dilution series are based on net peptide content,
277 calculated by multiplying the dry weight by %N and by purity. %N is a measure of the peptide
278 (rather than salt) fraction in the lyophilised product, while purity, provided by the manufacturer, is
279 the fraction of the peptide with the desired sequence among all supplied peptides. Peptide
280 sequences are listed in Table S7.
281

282 ## Statistical analysis

283 Chi^2 tests were used to analyse the distribution of peptides according to their functional group
284 among the different k-means clusters (Figure 1). Wilcoxon test for all paired comparaison with a
285 Holm correction were used to analyse the distributions of peptide features (Figure 2 and Figure 3).
286 One-way analysis of variance (ANOVA) and Tukey post-hoc were used to compare the Pearson
287 correlation coefficients to analyse fluorescence intensities (Supplementary Figure 9). A p-value
288 threshold of 0.05 was used for all tests. All statistical calculations were performed with the stats
289 package (v3.6.2) of the R version 3.6.1 and with functions from the Python scipy module (v1.2.3).
290

291 ## Code availability

292 All Python and R in-house scripts are available at
293 https://github.com/Clotildegarrido/Peptides_Analysis
294

295 # Results

296 ## TPs and HA-RAMPs share a common set of physico-chemical properties

297 *Peptide families and their descriptors*

298 We performed a comparative analysis of different functional groups of peptides
299 (Supplementary Table S1). We selected TPs from *Chlamydomonas reinhardtii*, *Arabidopsis*
300 *thaliana*, *Saccharomyces cerevisiae* and *Homo sapiens* for which both the subcellular location of
301 the cargo protein and the cleavage site have been experimentally determined (Supplementary Table
302 S2). We retrieved from the CAMP$_{R3}$ database [42] 31 HA-RAMP families with a documented
303 amphiphilic domain (see Material and Methods) and, as negative control, the cyclotide family of
304 globular AMPs (Supplementary Table S4). We also considered a set of peptides, hereafter referred
305 to as secretory signal peptides (SPs), which function as address tags, just as TPs do, but target a
306 different subcellular compartment. SPs have a well-established evolutionary link and all use Sec-
307 type translocation systems [66–68]. We retrieved as SPs the bacterial SPs (bSPs) that target
308 proteins for periplasmic secretion, their eukaryotic relatives (eSPs) targeting proteins to the
309 endoplasmic reticulum, and thylakoid SPs (tSPs), more commonly referred to as thylakoid transit
310 peptides, that target proteins to the thylakoids [6,68] (Supplementary Table S3). Lastly, we
311 generated a set of random peptides (Supplementary Table S5).

312 All peptides were less than 100 amino acids long. On average they are comprised of 45
313 residues for TPs, 32 residues for HA-RAMPs and 31 residues for SPs. Because TPs and HA-
314 RAMPs are short peptides with very limited sequence similarity, classical phylogenetic inferences
315 were not applicable [6]. Thus, to evaluate the likelihood of an evolutionary relationship between
316 TPs and HA-RAMPs, we resorted to their physico-chemical properties rather than to their primary
317 sequences and used the amino-acid descriptors 'Z-scales' defined by Hellberg [47]. Each of the 20
318 amino acids is therein described as a set of three values, which correspond to the first three linear
319 combinations (principal components) of 29 physico-chemical properties measured experimentally.
320 These three Z-scales reflect mostly hydrophobicity (z1), bulkiness of the side chain (z2) and
321 electronic properties (z3). A comparative study of 13 types of amino acid descriptors showed that
322 these three Z-scales are sufficient to explain the structure-activity variability of peptides [69,70].
323 To account for interdependencies between residues - i.e. the properties of the whole peptide - each
324 peptide was defined by 36 terms corresponding to auto-cross covariances (ACC) between Z-scale
325 values [48] within a 4-neighbor window, which mimics a single α-helix turn of 3.6 residues (see
326 "Peptide description" in the Materials and Methods section).
327
328 *HA-RAMPs can be divided into two distinct classes*
329 Many HA-RAMPs families have been defined on a rather descriptive basis in the literature
330 and the criteria used to group peptides differ from one family to another. To draw a more consistent
331 picture of the diversity of HA-RAMPs, we performed a k-means clustering of our 686 selected
332 HA-RAMPs, together with the 353 SPs and 433 TPs, based on the Euclidean distances between
333 their 36 ACC vectors (Figure 1A). Among clustering with k varying from 2 to 10, clustering with
334 k=2 gave the highest average of silhouette coefficients [51] for all peptides (reflecting the
335 consistency of the clustering). HA-RAMPs distributed between the two clusters in a 2/3 vs. 1/3
336 proportion (Figure 1B). The 68% of HA-RAMPs that grouped in cluster 1 will be hereafter referred
337 to as class I HA-RAMPs, whereas those in cluster 2 will be referred to as class II HA-RAMPs.
338 60% of the families described in the literature fitted well either into cluster 1 or cluster 2, which
339 supports their classification as families of distinct physico-chemical properties (Figure 1C).
340 However, 13 families contained peptides distributed in both clusters, calling for further
341 investigation of their identification as members of a same family.

To get a more detailed picture of their similarity relationships, we performed a neighbour-joining (NJ) clustering of all HA-RAMPs based on the Euclidean distances between their 36 ACC vectors (Supplementary Figure 2). The most external bipartitions of the clustering tree are highly supported, while internal ones are less supported. Class I and class II HA-RAMPs are not intermingled on that tree and tend to form robust homogeneous sub-clusters. When considering peptides according to their antimicrobial families described in the literature, their distribution along the tree was patchy (outer colour circle on Supplementary Figure 2).

To better handle the differences between class I and class II HA-RAMPs, we compared their features in terms of length, hydrophobicity, net charge and number of residues that can theoretically adopt an amphiphilic helical structure (Figure 2). The two classes indeed had rather distinctive traits: compared to class II HA-RAMPs, class I HA-RAMPs have significantly lower hydrophobicity (Figure 2A), higher net charge (Figure 2B), longer amphiphilic helices (Figure 2C) and are overall longer peptides (Figure 2D).

.

TPs and class I HA-RAMPs share a set of physico-chemical properties

Based on the k-means classification of HA-RAMPs in two classes with distinct traits, we further investigated the properties of TPs and SPs relative to those of HA-RAMPs. Figure 1 shows that all TPs, but a few isolated ones, clustered with class I HA-RAMPs. The majority of SPs grouped together in the other cluster. The grouping of most TPs with a large subset of class I HA-RAMPs proved very robust, being maintained for k values increasing up to 10 (Supplementary Figure 3). Moreover, when grouped together, class I HA-RAMPs and TPs are always the most abundant peptides in the cluster (the left one in Supplementary Figure 3). In contrast, the grouping of class II HA-RAMPs and SPs vanishes with increasing k values, being lost for k values greater than 6 (Supplementary Figure 3). These observations reveal strong similarities among a large subset of class I HA-RAMPs and TPs, but not between SPs and class II HA-RAMPs (see below).

The basis for this distinct clustering is documented in Figure 2: TPs and class I HA-RAMPs follow the same trends, away from the more hydrophobic class II HA-RAMPs and from SPs that bear a well-documented hydrophobic stretch (Figure 2A). Furthermore, TPs and class I HA-RAMPs all form amphiphilic helices of similar length (Figure 2C). Interestingly, randomly generated peptides contain amphiphilic stretches of similar length, albeit without the characteristic

373 cationic character of TPs and HA-RAMPs. By contrast, SPs and globular cyclotides contain
374 significantly shorter amphiphilic stretches, suggesting amphiphilicity may be actively selected
375 against. Shorter amphiphilic helices in class II HA-RAMPs are due to the shorter overall length of
376 these peptides (Figure 2D). The fact that cTPs are significantly longer than class I HA-RAMPs and
377 mTPs while containing amphiphilic stretches of similar length is in line with the idea that cTPs
378 contain additional sequence elements [5,36]. The control group of globular cyclotides display the
379 highest hydrophobicity (Figure 2A) and the shortest amphiphilic helices (Figure 2C), as expected
380 from their globular nature.
381 Because mTPs are well recognized as being of amphiphilic nature whereas cTPs are often referred
382 to as unstructured peptides, we carefully reassessed their amphiphilic properties in the various
383 organisms that we used in the present study (Figure 3). On average, cTPs and mTPs form
384 amphiphilic helices of similar length, but for *S. cerevisiae* mTPs which are much shorter (Figure
385 3A). Both mTPs and cTPs are longer in *A. thaliana* than in *C. reinhardtii*, which results in a higher
386 proportion of amphiphilic sequence in mTPs and cTPs from the latter (Figure 3C), in line with
387 previous reports that algal cTPs resemble plant mTPs [71]. However, irrespective of species, cTPs
388 are longer than mTPs, thus displaying smaller proportion of amphiphilic sequence. Taken together,
389 these characteristics explain why cTPs have been reported as less amphiphilic than mTPs, despite
390 the presence of a *bona fide* amphiphilic helix. It is of note that the amphiphilic helices detected in
391 random peptides have widely different characteristics since they also involve negatively charged
392 residues which are largely excluded from those detected in TPs and HA-RAMPs (Figure 1C and
393 3D): the majority of the amphipathic helices are positively charged in TPs (92%), when they are
394 only 47% of those identified among random peptides.
395 To better characterise the physico-chemical properties that are most discriminatory between
396 SPs, HA-RAMPs and TPs, we performed a Principal Component Analysis (PCA) of these peptides
397 described by their ACC vectors. Figure 4 presents a PCA without class II HA-RAMPs (see
398 Supplementary Figure 4 for a PCA with class II HA-RAMPs). The separation between all peptides
399 is provided by a combination of the contributions of various ACC terms to the two principal
400 components (PC1 and PC2). As shown by the contributions of the various ACC terms
401 (Supplementary Figure 5A), the terms reflecting the coupling between electronic and steric
402 properties of the residues from the opposite faces of the amphiphilic helix are the main contributors
403 to PC1 whereas the terms reflecting the hydrophobic and steric properties of the residues along the

404 same face of the helix mostly contribute to PC2. When considering the amphiphilic helical domain
405 of a peptide, these terms respectively reflect the electronic constraints that residues have to match
406 on the same face of the α-helix and the amphiphilic constraints between residues from opposite
407 faces.

408 The evolutionarily-linked and hydrophobic tSPs, bSPs and eSPs co-localise on the top of the
409 graph, away from TPs and class I HA-RAMPs (Figure 4). Class I HA-RAMPs occupy the bottom
410 of the graph with an amphiphilic gradient from left to right, overlapping with TPs on the left side.
411 TPs form a single overlapping spread, but mTPs show a tendency for higher values along PC1 than
412 cTPs, in agreement with amphiphilic helices taking up a higher proportion of each peptide in mTPs.
413 These observations are in line with k-means clustering (Figure 2, Supplementary Figure 3) where
414 TPs group with class I HA-RAMPs, apart from SPs. As control groups, we display on Figure 4 the
415 distribution of globular AMPs that occupy a separate part of the physico-chemical space to the left
416 of the graph, reflecting their widely different structure, despite a shared antimicrobial function. The
417 overlap of random peptides is higher with HA-RAMPs and TPs than with SPs. Note that part of
418 this overlap originates from amphiphilic features of random peptides which are born by negatively
419 charged residues, at variance with the positively charged amphiphilic helices present in TPs and
420 Class I HA-RAMP (Figure 3D).

421 When considering all HA-RAMPs together with SPs and TPs in the plane defined by PC1
422 and PC2 (Supplementary Figure 4A), TPs are almost completely enclosed within the convex area
423 of class I HA-RAMPs. The partial overlap of SPs with class II HA-RAMPs stems from their more
424 hydrophobic character, compared to class I HA-RAMPs. By contrast, in the plane defined by PC1
425 and PC3 (reflecting the hydrophobic properties of the residues along the same side of the helix),
426 class II HA-RAMPs group closer to class I HA-RAMPs and away from SPs (Supplementary Figure
427 4B) reflecting their different amphiphilic character (Supplementary Figure 4D). However, TPs still
428 overlap with class I HA-RAMPs in the PC1/PC3 plane, reflecting a much tighter physico-chemical
429 relatedness, as already observed when comparing the general features of the peptides (Figure 2)
430 and within k-means clustering (Supplementary Figure 3).

431

432 HA-RAMPs and TPs show dual targeting and antimicrobial activities

433 *A TP cleavage-site fragment is required for import of the Venus reporter*

434 To assess the targeting activity of AMPs we used a bicistronic expression system based on
435 ribosome re-initiation as described by Onishi and Pringle [58] with coding sequences for candidate
436 peptides inserted upstream of a Venus fluorescent reporter [72]. In this bicistronic system, the stop
437 codon of the fluorescent reporter and the initiation codon of the selectable marker are separated by
438 only six nucleotides (TAGCAT), which is sufficient to ensure robust expression of both genes in
439 *C. reinhardtii*. Compared to classical expression systems where the selectable marker is driven by
440 a separate promoter, bicistronic expression results in a much higher fraction of recovered
441 transformants showing expression of the gene of interest [58].
442 Mitochondria and chloroplasts were imaged respectively using a MitoTracker dye and
443 chlorophyll autofluorescence. In the absence of Venus (expression of the selectable marker only),
444 some crosstalk is visible in the Venus channel (Supplementary Figure 6A), which appears to
445 originate from thylakoid localised pigments and in particular from the eyespot. In the absence of a
446 presequence (Supplementary Figure 6B) Venus remains cytosolic.
447 Surprisingly, the fluorescent reporter was equally cytosolic when the Rubisco activase cTP
448 (RBCA-cTP) up to the cleavage site was included upstream of Venus (Supplementary Figure 6C).
449 For import into the chloroplast, a stretch of 23 downstream residues was required (RBCA-cTP+),
450 to reconstitute a native cleavage site (Supplementary Figure 6D). This finding is in line with
451 previous efforts to target reporters to the chloroplast [73,74]) and led us to include residues -10 to
452 +23 with respect to the cleavage site in subsequent constructs. This cleavage site fragment (RBCA-
453 cs) by itself displayed no capacity for directing the Venus reporter into either organelle
454 (Supplementary Figure 6E). We note that in addition to colocalising with chlorophyll, the Venus
455 reporter driven by RBCA-cTP+ was abundant around or within the pyrenoid, the native location
456 of RBCA (Supplementary Figure 6D). The pyrenoid is a proteinaceous structure of importance to
457 the algal carbon-concentrating mechanism that contains a lower density of thylakoid membranes
458 than the rest of the chloroplast. As a result, it is visible as a characteristic dark zone in chlorophyll
459 auto-fluorescence at the apex of the chloroplast [75], making Venus accumulating at this site easy
460 to spot. Mitochondrial localisation of Venus driven by a native *C. reinhardtii* mTP (CAG2-mTP+),
461 including post-cleavage site residues, is characterised by a tell-tale pattern [75] and co-localisation
462 with the MitoTracker signal (Supplementary Figure 6F). When the residues of this same mTP were
463 rearranged so as to impede the formation of an amphiphilic helix, the resulting peptide was no
464 longer able to target the reporter (Supplementary Figure 7A).

465

466 *HA-RAMPs target Venus to endosymbiotic organelles*

467 To assess the organelle targeting ability of HA-RAMPs, we selected five class I peptide
468 candidates that clustered with TPs, by k-means clustering based on their Euclidean distances:
469 bacillocin 1580 and enterocin HF from the bacteriocin IIA family, the cecropin sarcotoxin-1D,
470 brevinin-2ISb from the brevinin-2 family, and the well-studied magainin II. These candidates
471 localise next to TPs in our PCA analysis (Supplementary Figure 8A). When fused alongside
472 RBCA-cs upstream of Venus and expressed in *C. reinhardtii* (Figure 5), both bacillocin 1580
473 (Figure 5A) and enterocin HF (Figure 5B) give rise to a fluorescence signal that is co-localised
474 with chlorophyll auto-fluorescence, in line with their proximity to cTPs in the PCA (Supplementary
475 Figure 8A). There is also a marked accumulation around the pyrenoid, particularly for bacillocin
476 1580. Although closer to mTPs in our PCA analysis (Supplementary Figure 8A), sarcotoxin-1D
477 also targeted Venus to the chloroplast (Figure 5C), in line with the fact that some cTPs are found
478 in the vicinity of our sarcotoxin-1D construct (Supplementary Figure 8A). Brevinin-2Isb on the
479 other hand, proximal both to mTPs and cTPs in PCA, resulted in Venus fluorescence showing the
480 typical pattern of mitochondrial localisation, co-localising with the MitoTracker dye (Figure 5D).
481 Magainin II also targeted Venus to the mitochondria (Figure 5E), as might be expected from the
482 construct most distal to cTPs in our PCA (Supplementary Figure 8A). Class I HA-RAMPs are thus
483 capable of targeting a cargo protein to either type of endosymbiotic organelles.

484 By contrast, when fused to two peptides with computationally generated random amino acid
485 sequences followed by RBCA-cs, Venus fluorescence remained in the cytosol (Supplementary
486 Figure 7B,C), showing that random peptides do not necessarily generate targeting in the presence
487 of the RBCA-cs fragment. Furthermore, the class II HA-RAMP Brevinin 1E, fused to RBCA-cs,
488 equally failed to deliver Venus into either organelle, appearing instead to accumulate in the vicinity
489 of the chloroplast, particularly in one bright spot (Supplementary Figure 7D).

490 In order to demonstrate that the typical cells shown in Supplementary Figure 6 and Figure 5
491 are representative of the populations they were drawn from, we quantified co-localisation by
492 calculating Pearson correlation coefficients (PPC) across fluorescence channels [59] for around 30
493 cells per strain (Supplementary Figure 9). Cells expressing the CAG2-mTP+, magainin II and
494 brevinin-2ISb constructs had significantly higher PCCs between Venus and MitoTracker signals
495 than cells expressing any other constructs, confirming mitochondrial localisation of Venus.

496 Similarly, the RBCA-cTP+, bacillocin 1580, sarcotoxin-1D and enterocin HF constructs gave rise
497 to significantly higher PCCs between Venus and chlorophyll autofluorescence, indicating Venus
498 does indeed reside in the chloroplast. Since nuclear transformation in *C. reinhardtii* results in
499 random integration, we also checked that the genomic locus of integration did not influence
500 targeting: import phenotypes were consistent across three independent insertion lines
501 (Supplementary Figure 10).

502 For an independent assessment of Venus localisation, we isolated intact chloroplasts and
503 mitochondria from whole cells of *C. reinhardtii* harbouring one chloroplast and one mitochondrial
504 targeting construct (Figure 6). As previously described [60], chloroplast-enriched fractions still
505 show some mitochondrial contamination due to the presence of a subpopulation of mitochondria
506 firmly bound to chloroplasts in this microalga . In agreement with fluorescence imaging
507 observations, bacillocin 1580-driven Venus-FLAG was absent from isolated mitochondria but
508 present in whole-cell and chloroplast-fractions, just like the chloroplast markers OEE2 and RBCS
509 (Figure 6A). Magainin II-driven Venus-FLAG behaved like mitochondrial markers COXIIb and
510 F1β, being present in all three fractions (Figure 6B). Note that the mitochondrial fraction appears
511 underloaded, likely due to an overestimation of protein concentration. Nonetheless, the strong
512 FLAG signal in the whole cell fraction suggests that not all of the reporter protein is imported, in
513 line with some Venus fluorescence originating from the cytosol in this strain (Figure 5E,
514 Supplementary Figure 10K).

515 For both constructs, some of the Venus-FLAG reporter was protected from degradation by
516 proteinase K in isolated organelles unless treated with detergents, again mirroring the behaviour of
517 organelle-specific controls (Figure 6C, D). This confirms that bacillocin 1580 and magainin II act
518 as *bona fide* TPs, with a significant fraction of the cargo protein localised inside the respective
519 targeted organelle. A larger-sized fraction of Venus-FLAG did show sensitivity to proteinase K in
520 the absence of detergents. This sensitivity mirrored that of tubulin and BIP, both minor
521 contaminants in mitochondrial and chloroplast fractions respectively that are not protected within
522 organelles and digested readily irrespective of the presence of a detergent. Thus, a subpopulation
523 of AMP-reporter pre-proteins remains associated with the outer membrane of either organelle,
524 likely as a result of incomplete or aborted translocation.

525

526 *TPs show antimicrobial activity*

527 To determine the AMP-activity of TPs, we performed the symmetrical experiment. Several
528 chemically synthesised TPs, chosen for their variable proximity to class I HA-RAMPs
529 (Supplementary Figure 8B), were used to challenge *Bacillus subtilis* in a standard assay [65] using
530 magainin II as a positive control (Figure 7). *B. subtilis* was chosen as target organism rather than
531 *E. coli*, the other standard laboratory bacterial species, because it proved more sensitive to HA-
532 RAMP activity (Supplementary Figure 11). A high sensitivity was deemed a useful feature for an
533 antimicrobial assay in this proof-of-principle experiment, since we expected TPs to have a lower
534 activity than *bona fide* AMPs as they have been selected for targeting and not for impeding
535 microbial growth over the last 1.5 By. All four tested *C. reinhardtii* TPs showed antimicrobial
536 activity, as did F1β-mTP, the mTP of a mitochondrial ATP synthase subunit from *Neurospora*
537 *crassa*, whose antimicrobial activity had previously been reported [76]. By contrast, neither the *A.*
538 *thaliana* TL16-tSP, which targets proteins to the thylakoid lumen, nor the small hormone peptide
539 cholecystokinin-22 (cck-22), here used as negative controls, inhibited growth demonstrating that
540 antimicrobial activity is not simply an inherent feature shared by all peptides.

541 Discussion

542 *Diversity of HA-RAMPs*

543 In our *in silico* analysis, we first showed that HA-RAMPs can be grouped into distinct
544 subtypes that do not always line up with the classification into antimicrobial families described in
545 the literature (see Supplementary Text). Our analysis indicates that a systematic classification
546 according to physico-chemical properties would be possible upon further investigation, which
547 should prove of interest to the AMP community. However, it must be kept in mind that many
548 bipartitions along the NJ clustering tree still have limited support.
549

550 *Evidence for a common origin of TPs with a class of HA-RAMPs*

551 Our *in silico* and *in vivo* data support a common evolutionary origin of TPs and HA-RAMPs
552 [11] as they have similar physico-chemical properties and show cross-functionalities.

553 Whether by k-means clustering (whatever the k-values) or by PCA analysis on the three first
554 components, TPs consistently grouped together with class I HA-RAMPs and away from the three
555 types of SPs targeting to bacterial periplasm, ER or thylakoid compartments, further emphasising
556 their extensive similarities. These shared physico-chemical properties are consistent with an

557 evolutionary link between a large subset of class I HA-RAMPs and TPs. On the other hand, the
558 grouping of class II HA-RAMPs and SPs - being both more hydrophobic than TPs and class I HA-
559 RAMPS – is not robust in PCA and k-means analysis.

560 It had been argued that a fraction of random sequences (between 20 and 30% of those that
561 were tested) could function as mitochondrial or secretory targeting peptides [77–79]. The random
562 sequences that allowed functional targeting were strongly biased in sequence, with a requirement
563 for a positively charged amphiphilic helix for proper interaction with the membrane surface [33].
564 This is in line with our own observation of an overlap between some random peptides, class I HA-
565 RAMPs and TPs in our PCA analysis and with the shared properties of class I HA-RAMPs and
566 TPs.

567 While the presence of amphiphilic helices in mTPs is well-established [31,32], the
568 amphiphilic nature of cTPs had been questioned [37]. The present study shows that cTPs do display
569 amphiphilic stretches capable of folding into amphiphilic helices, in line with NMR studies on
570 selected cTPs in membrane-mimetic environments [38–40]. These helices are of similar length as
571 those of mTPs, but make up a shorter proportion of the peptide in longer cTPs. Their amphiphilic
572 character of cTPs may have been overlooked because the amphiphilic helix, which covers most of
573 the shorter mTP sequences, is surrounded by additional elements , which do not fold into
574 amphiphilic helices, such as an uncharged N-terminus [6,34–36] and a C-terminus with β-sheet
575 characteristics [5,6].

576 Beyond similarities in physico-chemical properties, the proposed evolutionary relationship
577 between TPs and HA-RAMPs was experimentally supported here by the antimicrobial activity
578 observed for all tested TPs (Figure 7). It is very remarkable that TPs still display an antimicrobial
579 activity, since they have not been selected for this function for the last 1.5 By [2]. It is not a surprise
580 then, that higher concentrations of TPs, relative to the *bona fide* AMP Magainin II, are required to
581 impede bacterial growth.

582 Further support for an evolutionary relationhip between these peptides stems from the organelle
583 targeting abilities of the five HA-RAMPs we probed experimentally, such as bacillocin 1580,
584 targeting the chloroplast, and magainin II, targeting the mitochondria (Figures 5 and 6). Our
585 experiments using HA-RAMP-and TP-driven targeting to organelles, argue for a similar import
586 process for both types of peptide through the canonical translocation pathways for mitochondria
587 (TOM/TIM for Translocase of the Outer/Inner Membrane) and chloroplast (TOC/TIC for

588 translocon on the outer/inner chloroplast membrane). Indeed, the Venus reporter is localised in the
589 stroma or matrix with a post-import cleavage of the N-terminal pre-sequences. By contrast, non-
590 canonical targeting, which has been identified in a very limited number of cases [80,81], including
591 a handful of glycoproteins [82], involves proteins that lack a cleavable pre-sequence and are
592 delivered to envelope compartments –outer or inner membrane, or inter-membrane space – but not
593 to the organelle interior [5,7,83].

594 One could argue that, rather than the present evolutionary scenario, a convergent evolution
595 of class I HA-RAMPs and TPs driven by strong selective constraints could have led these peptides
596 to adopt the same optimum in their physico-chemical properties. However, the respective
597 antimicrobial and intracellular targeting functions of class I HA-RAMPs and TPs do not *per se*
598 constitute a selective pressure for convergent evolution: as documented in the present study,
599 cyclotides globular AMPs, as well as class II HA-RAMPs are clearly distinct from class I HA-
600 RAMPs despite a shared antimicrobial function. Similarly, SPs function as cleavable N-terminal
601 targeting sequences like TPs but do not group with class I HA-RAMPs nor do they show
602 antimicrobial activity.

603

604 *Efficient targeting to extant organelles requires specific sequences besides the amphiphilic helix*
605 *of TPs*

606 Previous studies showed that short cTPs rely on the N-terminal region of the mature protein
607 to allow chloroplast targeting [73]. Accordingly, cTPs being shorter in Chlamydomonas than in
608 plants [this study and [71]], post-cleavage site residues are critical for proper chloroplast-targeting
609 in this alga, as we demonstrated here for RBCA. This prompted us to include RBCA post-cleavage
610 site residues in our HA-RAMP constructs. The mechanistic contribution of these mature N-termini
611 is still unclear, but they could provide an unfolded stretch long enough to elicit import [73].

612 A major issue in targeting to intracellular organelles in plants and algae is the ability of a
613 given presequence to avoid dual targeting. Several in vitro studies suggest that specific targeting is
614 achieved, at least in part, through competition between the two organelle import systems. For
615 instance, isolated mitochondria import cTPs [84,85] whereas, non-plants mTPs can drive import
616 into isolated chloroplasts [86,87]. To avoid miss-targeting, plant and algal TPs have probably
617 further evolved some specific traits of the N-terminal peptide region for targeting to chloroplasts
618 [34,88,89]. Targeting specificity has been improved further with the acquisition by mTPs of a

619 chloroplast avoidance signal consisting in multiple Arg at their N-terminus [36]. In agreement with
620 this proposal, we note that, among the chloroplast-targeting HA-RAMPs, Bacillocin 1580 carries
621 no charge within the first ten residues, and Enterocin HF carries a single Lys only. However,
622 Sarcotoxin 1D has four charged residues within this N-terminal window, including two Arginines
623 which might have been expected to exclude the construct from the chloroplast [36].

624 Other cTP motifs have been suggested to play some role in chloroplast protein import, such
625 as Hsp70 binding sites within the first 10 residues of the peptide [35,55], or FGLK motifs, grouping
626 aromatic (F), helix-breaking (G), small hydrophobic (L) and basic (K) residues for interaction with
627 TOC receptors [35,56]. Bacillocin 1580 indeed contains one FGLK-site (sensu [56]), but neither
628 enterocin HF, sarcotoxin-1D nor the RBCA presequence do, while the mitochondrial-targeting
629 magainin II contains two. Clearly, further work is needed to understand mitochondrial versus
630 chloroplast targeting for the HA-RAMPs under study.

631

632 *Targeting peptides and the translocation machinery*

633 Some bacterial Omp85 outer membrane assembly factors, which target proteins by a C-
634 terminal phenylalanine [90] and are thought to have given rise to TOC75, a core component of
635 TOC [91]. Since Rhodophyte and Glaucophyte cTPs start with a conserved phenylalanine [92],
636 chloroplast protein import could have benefited from a functional inversion of this cyanobacterial
637 protein in the evolution of the TOC complex. Although this observation was taken as an argument
638 against the emergence of cTPs from HA-RAMPs [93], we argue that HA-RAMPs would have
639 originally interacted with the outer membrane lipid headgroups [5], then crossed the outer
640 membrane spontaneously [94,95], with some HA-RAMPs also interacting with Omp85 proteins
641 [96]. In this view, the most likely evolutionary scenario for chloroplast import has involved
642 recruitment of Omp85 to improve delivery of HA-RAMP-tagged proteins to the import-and-
643 destroy receptor at the inner membrane surface.

644 The bacterial resistance apparatus at the origin of the chloroplast protein translocon, aimed
645 to prevent the lethal disruption of plasma membrane integrity by AMPs [22,23] is most likely to
646 be found in the TIC rather than the TOC part of the translocon. It should be emphasized that cTPs
647 have evolved in a context widely different from that prevailing for the emergence of mTPs. The
648 latter indeed appeared in absence of any pre-existing import system in the archeal ancestor of
649 eukaryotic cells. In contrast, the eukaryotic ancestor of Archeplastidia was in some way "pre-

650 adapted" for the recruitment of Class I HA-RAMP for import functions. This does not mean that
651 cTPs merely have recruited the TOM/TIM that form the protein channel as well as Tic21, Tic22,
652 Tic23, Tic32, Tic55 and Tic62 are of cyanobacterial origin [97–99]. However, we anticipate a
653 common origin of some TIC and TIM subunits which will require an extensive phylogenetic
654 analysis of the two sets of translocon components.
655
656 *Conclusion*
657 Although evolutionary scenarios necessarily give rise to conflicting views, it should be kept in
658 mind that neither the scenario of convergent evolution nor that of a spontaneous generation of TPs
659 account for the emergence of the ancestral mitochondrial and chloroplast translocation systems. In
660 contrast, an antimicrobial origin of TPs is a more parsimonious scenario, in which the import-and-
661 destroy ancestral mechanism allowing the endosymbiont to resist the attacks of AMPs [20–26] is
662 at the root of the translocation systems [11]. Further support for this view came from recent studies
663 of the amoeba *Paulinella chromatophora*, which acquired a novel primary endosymbiotic organelle
664 called "chromatophore" approximately 100 million years ago [100]. Proteomic analysis of these
665 chromatophores identified a large set of imported AMP-like peptides as well as chromatophore-
666 imported proteins harbouring common N-terminal sequences containing AMP-like motifs [101].
667 These findings thus provide an independent example of a third primary endosymbiosis that is
668 accompanied by the evolution of an AMP-derived protein import process. The detailed
669 evolutionary histories of extant organelle translocons and bacterial transmembrane channels
670 involved in AMP-resistance mechanisms should provide a means to further assess the antimicrobial
671 origin of organelle-targeting peptides.

672 Acknowledgments

673 We thank Richard Kuras, Ulrike Endesfelder, Michael Schroda and Moritz Meyer for
674 fruitful discussions and advice, Masayuki Onishi and the Pringle lab, for sharing their bi-cistronic
675 expression plasmids, Pierre Crozet for advice on plasmid design, Zhou Xu and Simon Desjardin
676 for help with microscopy, and Barry Bruce and Prakitchai Chotewutmontri for their help in the
677 correct implementation of Hsp70 binding site and FGLK motif search scripts. This work was
678 supported by the annual funding from the Centre National de la Recherche Scientifique and
679 Sorbonne University to UMR 7141, by the ChloroMitoRAMP ANR grant (ANR-19-CE13-0009)

and by LabEx Dynamo (ANR-LABX-011). ODC was supported by The Rothschild Foundation, the Labex dynamo and the ChloroMitoRAMP grant. CG was supported by the MATHTEST ANR grant (ANR-18-CE13-0027).

References

1. Martin, W.F.; Garg, S.; Zimorski, V. Endosymbiotic theories for eukaryote origin. *Philos Trans R Soc Lond B Biol Sci* **2015**, *370*, doi:10.1098/rstb.2014.0330.
2. Archibald, J.M. Endosymbiosis and Eukaryotic Cell Evolution. *Current Biology* **2015**, *25*, R911–R921, doi:10.1016/j.cub.2015.07.055.
3. Timmis, J.N.; Ayliffe, M.A.; Huang, C.Y.; Martin, W. Endosymbiotic gene transfer: organelle genomes forge eukaryotic chromosomes. *Nat Rev Genet* **2004**, *5*, 123–135, doi:10.1038/nrg1271.
4. Neupert, W.; Herrmann, J.M. Translocation of proteins into mitochondria. *Annual Review of Biochemistry* **2007**, *76*, 723–49, doi:10.1080/152165401753366096.
5. Chotewutmontri, P.; Holbrook, K.; Bruce, B.D. Chapter Six - Plastid Protein Targeting: Preprotein Recognition and Translocation. In *International Review of Cell and Molecular Biology*; Galluzzi, L., Ed.; Academic Press, 2017; Vol. 330, pp. 227–294.
6. von Heijne, G.; Steppuhn, J.; Herrmann, R.G. Domain structure of mitochondrial and chloroplast targeting peptides. *Eur. J. Biochem.* **1989**, *180*, 535–545.
7. Wiedemann, N.; Pfanner, N. Mitochondrial Machineries for Protein Import and Assembly. *Annual Review of Biochemistry* **2017**, *86*, 685–714, doi:10.1146/annurev-biochem-060815-014352.
8. Nakai, M. New Perspectives on Chloroplast Protein Import. *Plant Cell Physiol* **2018**, *59*, 1111–1119, doi:10.1093/pcp/pcy083.
9. Fukasawa, Y.; Oda, T.; Tomii, K.; Imai, K. Origin and Evolutionary Alteration of the Mitochondrial Import System in Eukaryotic Lineages. *Mol Biol Evol* **2017**, *34*, 1574–1586, doi:10.1093/molbev/msx096.
10. Reumann, S.; Inoue, K.; Keegstra, K. Evolution of the general protein import pathway of plastids (review). *Molecular Membrane Biology* **2005**, *22*, 73–86.
11. Wollman, F.-A. An antimicrobial origin of transit peptides accounts for early endosymbiotic events. *Traffic* **2016**, *17*, 1322–1328, doi:10.1111/tra.12446.
12. Maróti, G.; Kereszt, A.; Kondorosi, É.; Mergaert, P.; Maro, G. Natural roles of antimicrobial peptides in microbes , plants and animals. *Research in Microbiology* **2011**, *162*, 363–374, doi:10.1016/j.resmic.2011.02.005.
13. Besse, A.; Peduzzi, J.; Rebuffat, S.; Carré-Mlouka, A. Antimicrobial peptides and proteins in the face of extremes: Lessons from archaeocins. *Biochimie* **2015**, *118*, 344–355, doi:10.1016/j.biochi.2015.06.004.
14. Mergaert, P.; Kikuchi, Y.; Shigenobu, S.; Nowack, E.C.M. Metabolic Integration of Bacterial Endosymbionts through Antimicrobial Peptides. *Trends in Microbiology* **2017**, *25*, 703–712, doi:10.1016/j.tim.2017.04.007.
15. Mergaert, P. Role of antimicrobial peptides in controlling symbiotic bacterial populations. *Nat Prod Rep* **2018**, *35*, 336–356, doi:10.1039/c7np00056a.
16. Ball, S.G.; Bhattacharya, D.; Weber, A.P.M. Pathogen to powerhouse. *Science* **2016**, *351*,

723 659–60.
724 17. Zachar, I.; Szathmáry, E. Breath-giving cooperation: critical review of origin of
725 mitochondria hypotheses. *Biology Direct* **2017**, *12*, 19, doi:10.1186/s13062-017-0190-5.
726 18. Andersson, S.G.E.; Zomorodipour, A.; Andersson, J.O.; Sicheritz-Pontén, T.; Alsmark,
727 U.C.M.; Podowski, R.M.; Näslund, A.K.; Eriksson, A.-S.; Winkler, H.H.; Kurland, C.G. The
728 genome sequence of Rickettsia prowazekii and the origin of mitochondria. *Nature* **1998**, *396*,
729 133–140, doi:10.1038/24094.
730 19. Andrä, J.; Herbst, R.; Leippe, M. Amoebapores, archaic effector peptides of protozoan
731 origin, are discharged into phagosomes and kill bacteria by permeabilizing their membranes.
732 *Developmental and Comparative Immunology* **2003**, *27*, 291–304, doi:10.1016/S0145-
733 305X(02)00106-4.
734 20. Mason, K.M.; Bruggeman, M.E.; Munson, R.S.; Bakaletz, L.O. The non-typeable
735 Haemophilus influenzae Sap transporter provides a mechanism of antimicrobial peptide
736 resistance and SapD-dependent potassium acquisition. *Molecular Microbiology* **2006**, *62*, 1357–
737 1372, doi:10.1111/j.1365-2958.2006.05460.x.
738 21. Hiron, A.; Falord, M.; Valle, J.; Débarbouillé, M.; Msadek, T. Bacitracin and nisin
739 resistance in Staphylococcus aureus: a novel pathway involving the BraS/BraR two-component
740 system (SA2417/SA2418) and both the BraD/BraE and VraD/VraE ABC transporters. *Molecular*
741 *Microbiology* **2011**, *81*, 602–622, doi:10.1111/j.1365-2958.2011.07735.x.
742 22. Shelton, C.L.; Raffel, F.K.; Beatty, W.L.; Johnson, S.M.; Mason, K.M. Sap transporter
743 mediated import and subsequent degradation of antimicrobial peptides in Haemophilus. *PLoS*
744 *Pathogens* **2011**, *7*, e1002360, doi:10.1371/journal.ppat.1002360.
745 23. Rinker, S.D.; Gu, X.; Fortney, K.R.; Zwickl, B.W.; Katz, B.P.; Janowicz, D.M.; Spinola,
746 S.M.; Bauer, M.E. Permeases of the Sap Transporter Are Required for Cathelicidin Resistance
747 and Virulence of Haemophilus ducreyi in Humans. *J Infect Dis* **2012**, *206*, 1407–1414,
748 doi:10.1093/infdis/jis525.
749 24. Runti, G.; Lopez Ruiz, M. del C.; Stoilova, T.; Hussain, R.; Jennions, M.; Choudhury,
750 H.G.; Benincasa, M.; Gennaro, R.; Beis, K.; Scocchi, M. Functional characterization of SbmA, a
751 bacterial inner membrane transporter required for importing the antimicrobial peptide Bac7(1-
752 35). *J. Bacteriol.* **2013**, *195*, 5343–5351, doi:10.1128/JB.00818-13.
753 25. Guefrachi, I.; Pierre, O.; Timchenko, T.; Alunni, B.; Barrière, Q.; Czernic, P.; Villaécija-
754 Aguilar, J.-A.; Verly, C.; Bourge, M.; Fardoux, J.; et al. Bradyrhizobium BclA Is a Peptide
755 Transporter Required for Bacterial Differentiation in Symbiosis with Aeschynomene Legumes.
756 *MPMI* **2015**, *28*, 1155–1166, doi:10.1094/MPMI-04-15-0094-R.
757 26. Wang, Z.; Bie, P.; Cheng, J.; Lu, L.; Cui, B.; Wu, Q. The ABC transporter YejABEF is
758 required for resistance to antimicrobial peptides and the virulence of Brucella melitensis. *Sci Rep*
759 **2016**, *6*, 1–10, doi:10.1038/srep31876.
760 27. Ford Doolittle, W. You are what you eat: a gene transfer ratchet could account for
761 bacterial genes in eukaryotic nuclear genomes. *Trends in Genetics* **1998**, *14*, 307–311,
762 doi:10.1016/S0168-9525(98)01494-2.
763 28. Clarke, M.; Lohan, A.J.; Liu, B.; Lagkouvardos, I.; Roy, S.; Zafar, N.; Bertelli, C.;
764 Schilde, C.; Kianianmomeni, A.; Bürglin, T.R.; et al. Genome of Acanthamoeba castellanii
765 highlights extensive lateral gene transfer and early evolution of tyrosine kinase signaling.
766 *Genome Biology* **2013**, *14*, R11, doi:10.1186/gb-2013-14-2-r11.
767 29. Bechinger, B.; Zasloff, M.; Opella, S.J. Structure and orientation of the antibiotic peptide
768 magainin in membranes by solid-state nuclear magnetic resonance spectroscopy. *Protein Science*
769 **1993**, *2*, 2077–2084.

30. Bechinger, B. The structure, dynamics and orientation of antimicrobial peptides in membranes by multidimensional solid-state NMR spectroscopy. *Biochimica et biophysica acta* **1999**, *1462*, 157–83.
31. Roise, D.; Horvath, S.J.; Tomich, J.M.; Richards, J.H.; Schatz, G. A chemically synthesized pre-sequence of an imported mitochondrial protein can form an amphiphilic helix and perturb natural and artificial phospholipid bilayers. *EMBO J.* **1986**, *5*, 1327–1334.
32. Roise, D.; Theiler, F.; Horvath, S.J.; Tomich, J.M.; Richards, J.H.; Allison, D.S.; Schatz, G. Amphiphilicity is essential for mitochondrial presequence function. *The EMBO journal* **1988**, *7*, 649–53.
33. Lemire, B.D.; Fankhauser, C.; Baker, A.; Schatz, G. The mitochondrial targeting function of randomly generated peptide sequences correlates with predicted helical amphiphilicity. *J. Biol. Chem.* **1989**, *264*, 20206–20215.
34. Bhushan, S.; Kuhn, C.; Berglund, A.K.; Roth, C.; Glaser, E. The role of the N-terminal domain of chloroplast targeting peptides in organellar protein import and miss-sorting. *FEBS letters* **2006**, *580*, 3966–72, doi:10.1016/j.febslet.2006.06.018.
35. Chotewutmontri, P.; Bruce, B.D. Non-native, N-terminal Hsp70 molecular motor recognition elements in transit peptides support plastid protein translocation. *The Journal of biological chemistry* **2015**, *290*, 7602–21, doi:10.1074/jbc.M114.633586.
36. Lee, D.W.; Lee, S.; Lee, J.; Woo, S.; Razzak, M.A.; Vitale, A.; Hwang, I. Molecular mechanism of protein import specificity to chloroplasts and mitochondria in plant cells. *Mol Plant* **2019**, doi:10.1016/j.molp.2019.03.003.
37. von Heijne, G.; Nishikawa, K. Chloroplast transit peptides. The perfect random coil? *FEBS letters* **1991**, *278*, 1–3, doi:10.1016/0014-5793(91)80069-f.
38. Lancelin, J.M.; Bally, I.; Arlaud, G.J.; Blackledge, M.; Gans, P.; Stein, M.; Jacquot, J.P. NMR structures of ferredoxin chloroplastic transit peptide from Chlamydomonas reinhardtii promoted by trifluoroethanol in aqueous solution. *FEBS letters* **1994**, *343*, 261–6.
39. Krimm, I.; Gans, P.; Hernandez, J.F.; Arlaud, G.J.; Lancelin, J.M. A coil-helix instead of a helix-coil motif can be induced in a chloroplast transit peptide from Chlamydomonas reinhardtii. *European journal of biochemistry* **1999**, *265*, 171–80.
40. Wienk, H.L.; Wechselberger, R.W.; Czisch, M.; de Kruijff, B. Structure, dynamics, and insertion of a chloroplast targeting peptide in mixed micelles. *Biochemistry* **2000**, *39*, 8219–27.
41. Bruce, B.D. The paradox of plastid transit peptides: conservation of function despite divergence in primary structure. *Biochimica et Biophysica Acta (BBA) - Molecular Cell Research* **2001**, *1541*, 2–21, doi:10.1016/S0167-4889(01)00149-5.
42. Waghu, F.H.; Barai, R.S.; Gurung, P.; Idicula-Thomas, S. CAMPR3: A database on sequences, structures and signatures of antimicrobial peptides. *Nucleic Acids Research* **2016**, *44*, D1094–D1097, doi:10.1093/nar/gkv1051.
43. Berman, H.M.; Westbrook, J.; Feng, Z.; Gilliland, G.; Bhat, T.N.; Weissig, H.; Shindyalov, I.N.; Bourne, P.E. The Protein Data Bank. *Nucleic Acids Res* **2000**, *28*, 235–242, doi:10.1093/nar/28.1.235.
44. Rea, M.; Ross, R.; Cotter, D.; Hill, C. Part II Classification of Prokaryotic Antimicrobial Peptides, Chapter 3 Classification of Bacteriocins from Gram-Positive Bacteria. In *Prokaryotic antimicrobial peptides: from genes to applications*; Springer, 2011.
45. Hammami, R.; Zouhir, A.; Le Lay, C.; Ben Hamida, J.; Fliss, I. BACTIBASE second release: a database and tool platform for bacteriocin characterization. *BMC Microbiology* **2010**, *10*, 22, doi:10.1186/1471-2180-10-22.
46. Mookherjee, N.; Brown, K.L.; Hancock, R.E.W. Chapter 15 - Cathelicidins. In *Handbook*

817 *of Biologically Active Peptides (Second Edition)*; Kastin, A.J., Ed.; Academic Press: Boston,
818 2013; pp. 77–84 ISBN 978-0-12-385095-9.
819 47. Hellberg, S.; Sjoestroem, M.; Skagerberg, B.; Wold, S. Peptide quantitative structure-
820 activity relationships, a multivariate approach. *J. Med. Chem.* **1987**, *30*, 1126–1135,
821 doi:10.1021/jm00390a003.
822 48. Wold, S.; Jonsson, J.; Sjörström, M.; Sandberg, M.; Rännar, S. DNA and peptide
823 sequences and chemical processes multivariately modelled by principal component analysis and
824 partial least-squares projections to latent structures. *Analytica Chimica Acta* **1993**, *277*, 239–253,
825 doi:10.1016/0003-2670(93)80437-P.
826 49. Fauchère, J.-L.; Pliska, V. Hydrophobic parameters πof amino-acid side chains from the
827 partitioning of N-acetyl-amino-acid amides. *Eur. J. Med. Chem.* **1983**, *18*, 369–375.
828 50. Gautier, R.; Douguet, D.; Antonny, B.; Drin, G. HELIQUEST: a web server to screen
829 sequences with specific alpha-helical properties. *Bioinformatics* **2008**, *24*, 2101–2102,
830 doi:10.1093/bioinformatics/btn392.
831 51. Rousseeuw, P.J. Silhouettes: A graphical aid to the interpretation and validation of cluster
832 analysis. *Journal of Computational and Applied Mathematics* **1987**, *20*, 53–65,
833 doi:10.1016/0377-0427(87)90125-7.
834 52. Salichos, L.; Stamatakis, A.; Rokas, A. Novel Information Theory-Based Measures for
835 Quantifying Incongruence among Phylogenetic Trees. *Mol Biol Evol* **2014**, msu061,
836 doi:10.1093/molbev/msu061.
837 53. Stamatakis, A. RAxML Version 8: A tool for Phylogenetic Analysis and Post-Analysis of
838 Large Phylogenies. *Bioinformatics* **2014**, btu033, doi:10.1093/bioinformatics/btu033.
839 54. Letunic, I.; Bork, P. Interactive Tree Of Life (iTOL) v4: recent updates and new
840 developments. *Nucleic Acids Res* **2019**, *47*, W256–W259, doi:10.1093/nar/gkz239.
841 55. Ivey, R.A., 3rd; Subramanian, C.; Bruce, B.D. Identification of a Hsp70 recognition
842 domain within the rubisco small subunit transit peptide. *Plant physiology* **2000**, *122*, 1289–99.
843 56. Chotewutmontri, P.; Reddick, L.E.; McWilliams, D.R.; Campbell, I.M.; Bruce, B.D.
844 Differential transit peptide recognition during preprotein binding and translocation into flowering
845 plant plastids. *The Plant cell* **2012**, *24*, 3040–59, doi:10.1105/tpc.112.098327.
846 57. Harris, E. *The Chlamydomonas Sourcebook - 1st Edition*; Academic Press: San Diego,
847 1989; ISBN 978-1-4832-8860-4.
848 58. Onishi, M.; Pringle, J.R. Robust Transgene Expression from Bicistronic mRNA in the
849 Green Alga Chlamydomonas reinhardtii. *G3 (Bethesda, Md.)* **2016**, *6*, 4115–4125,
850 doi:10.1534/g3.116.033035.
851 59. Dunn, K.W.; Kamocka, M.M.; McDonald, J.H. A practical guide to evaluating
852 colocalization in biological microscopy. *American Journal of Physiology-Cell Physiology* **2011**,
853 *300*, C723–C742, doi:10.1152/ajpcell.00462.2010.
854 60. Willmund, F.; Schroda, M. HEAT SHOCK PROTEIN 90C is a bona fide Hsp90 that
855 interacts with plastidic HSP70B in Chlamydomonas reinhardtii. *Plant physiology* **2005**, *138*,
856 2310–22, doi:10.1104/pp.105.063578.
857 61. Craige, B.; Brown, J.M.; Witman, G.B. Isolation of chlamydomonas flagella. *Current*
858 *Protocols in Cell Biology* **2013**, 1–9, doi:10.1002/0471143030.cb0341s59.
859 62. Chua, N.H.; Blomberg, F. Immunochemical studies of thylakoid membrane polypeptides
860 from spinach and Chlamydomonas reinhardtii. A modified procedure for crossed
861 immunoelectrophoresis of dodecyl sulfate.protein complexes. *J. Biol. Chem.* **1979**, *254*, 215–223.
862 63. de Vitry, C.; Olive, J.; Drapier, D.; Recouvreur, M.; Wollman, F.A. Posttranslational
863 events leading to the assembly of photosystem II protein complex: a study using photosynthesis

mutants from Chlamydomonas reinhardtii. *Journal of Cell Biology* **1989**, *109*, 991–1006, doi:10.1083/jcb.109.3.991.

64. Whitney, S.M.; John Andrews, T. The gene for the ribulose-1,5-bisphosphate carboxylase/ oxygenase (Rubisco) small subunit relocated to the plastid genome of tobacco directs the synthesis of small subunits that assemble into Rubisco. *Plant Cell* **2001**, *13*, 193–205, doi:10.1105/tpc.13.1.193.

65. Wiegand, I.; Hilpert, K.; Hancock, R.E.W. Agar and broth dilution methods to determine the minimal inhibitory concentration (MIC) of antimicrobial substances. *Nature Protocols* **2008**, *3*, 163–175, doi:10.1038/nprot.2007.521.

66. von Heijne, G. The signal peptide. *The Journal of Membrane Biology* **1990**, *115*, 195–201, doi:10.1007/BF01868635.

67. Frain, K.M.; Gangl, D.; Jones, A.; Zedler, J.A.Z.; Robinson, C. Protein translocation and thylakoid biogenesis in cyanobacteria. *Biochimica et Biophysica Acta (BBA) - Bioenergetics* **2016**, *1857*, 266–273, doi:10.1016/j.bbabio.2015.08.010.

68. Schatz, G.; Dobberstein, B. Common Principles of Protein Translocation Across Membranes. *Science* **1996**, *271*, 1519–1526, doi:10.1126/science.271.5255.1519.

69. van Westen, G.J.; Swier, R.F.; Wegner, J.K.; IJzerman, A.P.; van Vlijmen, H.W.; Bender, A. Benchmarking of protein descriptor sets in proteochemometric modeling (part 1): comparative study of 13 amino acid descriptor sets. *J Cheminform* **2013**, *5*, 41, doi:10.1186/1758-2946-5-41.

70. van Westen, G.J.; Swier, R.F.; Cortes-Ciriano, I.; Wegner, J.K.; Overington, J.P.; IJzerman, A.P.; van Vlijmen, H.W.; Bender, A. Benchmarking of protein descriptor sets in proteochemometric modeling (part 2): modeling performance of 13 amino acid descriptor sets. *Journal of Cheminformatics* **2013**, *5*, 42, doi:10.1186/1758-2946-5-42.

71. Franzen, L.G.; Rochaix, J.D.; von Heijne, G. Chloroplast transit peptides from the green alga Chlamydomonas reinhardtii share features with both mitochondrial and higher plant chloroplast presequences. *FEBS Letters* **1990**, *260*, 165–168.

72. Nagai, T.; Ibata, K.; Park, E.S.; Kubota, M.; Mikoshiba, K.; Miyawaki, A. A variant of yellow fluorescent protein with fast and efficient maturation for cell-biological applications. *Nature biotechnology* **2002**, *20*, 87–90, doi:10.1038/nbt0102-87.

73. Bionda, T.; Tillmann, B.; Simm, S.; Beilstein, K.; Ruprecht, M.; Schleiff, E. Chloroplast import signals: the length requirement for translocation in vitro and in vivo. *Journal of molecular biology* **2010**, *402*, 510–23, doi:10.1016/j.jmb.2010.07.052.

74. Razzak, A.; Lee, D.W.; Yoo, Y.; Hwang, I. Evolution of rubisco complex small subunit transit peptides from algae to plants. *Scientific Reports* **2017**, *7*, 9279, doi:10.1038/s41598-017-09473-x.

75. Mackinder, L.C.M.; Chen, C.; Leib, R.D.; Patena, W.; Blum, S.R.; Rodman, M.; Ramundo, S.; Adams, C.M.; Jonikas, M.C. A Spatial Interactome Reveals the Protein Organization of the Algal CO2-Concentrating Mechanism. *Cell* **2017**, *171*, 133–147, doi:10.1016/j.cell.2017.08.044.

76. Hugosson, M.; Andreu, D.; Boman, H.G.; Glaser, E. Antibacterial peptides and mitochonrial presequences affect mitochonrial coupling, respiration and protein import. *European Journal of Biochemistry* **1994**, *223*, 1027–1033, doi:10.1111/j.1432-1033.1994.tb19081.x.

77. Baker, A.; Schatz, G. Sequences from a prokaryotic genome or the mouse dihydrofolate reductase gene can restore the import of a truncated precursor protein into yeast mitochondria. *Proceedings of the National Academy of Sciences* **1987**, *84*, 3117–3121, doi:10.1073/pnas.84.10.3117.

78. Dunn, C.D.; Paavilainen, V.O. Wherever I may roam: organellar protein targeting and evolvability. *Current Opinion in Genetics & Development* **2019**, *58–59*, 9–16, doi:10.1016/j.gde.2019.07.012.
79. Kaiser, C.A.; Preuss, D.; Grisafi, P.; Botstein, D. Many random sequences functionally replace the secretion signal sequence of yeast invertase. *Science* **1987**, *235*, 312–317, doi:10.1126/science.3541205.
80. Miras, S.; Salvi, D.; Piette, L.; Seigneurin-Berny, D.; Grunwald, D.; Reinbothe, C.; Joyard, J.; Reinbothe, S.; Rolland, N. Toc159- and Toc75-independent import of a transit sequence-less precursor into the inner envelope of chloroplasts. *The Journal of biological chemistry* **2007**, *282*, 29482–92, doi:10.1074/jbc.M611112200.
81. Moyet, L.; Salvi, D.; Bouchnak, I.; Miras, S.; Perrot, L.; Seigneurin-Berny, D.; Kuntz, M.; Rolland, N. Calmodulin is involved in the dual subcellular location of two chloroplast proteins. *The Journal of biological chemistry* **2019**, *294*, 17543–17554, doi:10.1074/jbc.RA119.010846.
82. Baslam, M.; Oikawa, K.; Kitajima-Koga, A.; Kaneko, K.; Mitsui, T. Golgi-to-plastid trafficking of proteins through secretory pathway: Insights into vesicle-mediated import toward the plastids. *Plant Signaling & Behavior* **2016**, *11*, e1221558, doi:10.1080/15592324.2016.1221558.
83. Villarejo, A.; Buren, S.; Larsson, S.; Dejardin, A.; Monne, M.; Rudhe, C.; Karlsson, J.; Jansson, S.; Lerouge, P.; Rolland, N.; et al. Evidence for a protein transported through the secretory pathway en route to the higher plant chloroplast. *Nat Cell Biol* **2005**, *7*, 1224–31.
84. Hurt, E.C.; Soltanifar, N.; Goldschmidt-Clermont, M.; Rochaix, J.D.; Schatz, G. The cleavable pre-sequence of an imported chloroplast protein directs attached polypeptides into yeast mitochondria. *The EMBO journal* **1986**, *5*, 1343–50.
85. Cleary, S.P.; Tan, F.C.; Nakrieko, K.A.; Thompson, S.J.; Mullineaux, P.M.; Creissen, G.P.; von Stedingk, E.; Glaser, E.; Smith, A.G.; Robinson, C. Isolated plant mitochondria import chloroplast precursor proteins in vitro with the same efficiency as chloroplasts. *The Journal of biological chemistry* **2002**, *277*, 5562–9, doi:10.1074/jbc.M106532200.
86. Huang, J.; Hack, E.; Thornburg, R.W.; Myers, A.M. A yeast mitochondrial leader peptide functions in vivo as a dual targeting signal for both chloroplasts and mitochondria. *The Plant cell* **1990**, *2*, 1249–60, doi:10.1105/tpc.2.12.1249.
87. Rödiger, A.; Baudisch, B.; Langner, U.; Klösgen, R.B. Dual targeting of a mitochondrial protein: the case study of cytochrome c1. *Molecular plant* **2011**, *4*, 679–87, doi:10.1093/mp/ssr001.
88. Ge, C.; Spanning, E.; Glaser, E.; Wieslander, A. Import determinants of organelle-specific and dual targeting peptides of mitochondria and chloroplasts in Arabidopsis thaliana. *Molecular plant* **2014**, *7*, 121–36, doi:10.1093/mp/sst148.
89. McKinnon, L.; Theg, S.M. Determinants of the Specificity of Protein Targeting to Chloroplasts or Mitochondria. *Molecular plant* **2019**, *12*, 893–895, doi:10.1016/j.molp.2019.05.004.
90. Robert, V.; Volokhina, E.B.; Senf, F.; Bos, M.P.; Van Gelder, P.; Tommassen, J. Assembly factor Omp85 recognizes its outer membrane protein substrates by a species-specific C-terminal motif. *PLoS Biol.* **2006**, *4*, e377, doi:10.1371/journal.pbio.0040377.
91. Sommer, M.S.; Daum, B.; Gross, L.E.; Weis, B.L.M.; Mirus, O.; Abram, L.; Maier, U.-G.; Kühlbrandt, W.; Schleiff, E. Chloroplast Omp85 proteins change orientation during evolution. *PNAS* **2011**, *108*, 13841–13846, doi:10.1073/pnas.1108626108.
92. Wunder, T.; Martin, R.; Löffelhardt, W.; Schleiff, E.; Steiner, J.M. The invariant phenylalanine of precursor proteins discloses the importance of Omp85 for protein translocation

958 into cyanelles. *BMC Evol Biol* **2007**, *7*, 236, doi:10.1186/1471-2148-7-236.
959 93. Knopp, M.; Garg, S.G.; Handrich, M.; Gould, S.B. Major Changes in Plastid Protein
960 Import and the Origin of the Chloroplastida. *iScience* **2020**, *23*, 100896,
961 doi:10.1016/j.isci.2020.100896.
962 94. Sato, H.; Feix, J.B. Peptide–membrane interactions and mechanisms of membrane
963 destruction by amphipathic α-helical antimicrobial peptides. *Biochimica et Biophysica Acta*
964 *(BBA) - Biomembranes* **2006**, *1758*, 1245–1256, doi:10.1016/j.bbamem.2006.02.021.
965 95. Piers, K.L.; Brown, M.H.; Hancock, R.E. Improvement of outer membrane-
966 permeabilizing and lipopolysaccharide-binding activities of an antimicrobial cationic peptide by
967 C-terminal modification. *Antimicrob. Agents Chemother.* **1994**, *38*, 2311–2316,
968 doi:10.1128/aac.38.10.2311.
969 96. Vimala, A.; Ramakrishnan, C.; Gromiha, M.M. Identifying a potential receptor for the
970 antibacterial peptide of sponge Axinella donnani endosymbiont. *Gene* **2015**, *566*, 166–174,
971 doi:10.1016/j.gene.2015.04.070.
972 97. Tripp, J.; Hahn, A.; Koenig, P.; Flinner, N.; Bublak, D.; Brouwer, E.M.; Ertel, F.; Mirus,
973 O.; Sinning, I.; Tews, I.; et al. Structure and conservation of the periplasmic targeting factor
974 Tic22 protein from plants and cyanobacteria. *The Journal of biological chemistry* **2012**, *287*,
975 24164–73, doi:10.1074/jbc.M112.341644.
976 98. Shi, L.; Theg, S. The chloroplast protein import system: from algae to trees. *Biochim*
977 *Biophys Acta.* **2013**, *1833*, 314–331.
978 99. Brouwer, E.M.; Ngo, G.; Yadav, S.; Ladig, R.; Schleiff, E. Tic22 from Anabaena sp. PCC
979 7120 with holdase function involved in outer membrane protein biogenesis shuttles between
980 plasma membrane and Omp85. *Molecular microbiology* **2019**, doi:10.1111/mmi.14222.
981 100. Delaye, L.; Valadez-Cano, C.; Pérez-Zamorano, B. How Really Ancient Is Paulinella
982 Chromatophora? *PLoS Curr* **2016**, *8*,
983 doi:10.1371/currents.tol.e68a099364bb1a1e129a17b4e06b0c6b.
984 101. Singer, A.; Poschmann, G.; Mühlich, C.; Valadez-Cano, C.; Hänsch, S.; Hüren, V.;
985 Rensing, S.A.; Stühler, K.; Nowack, E.C.M. Massive Protein Import into the Early-Evolutionary-
986 Stage Photosynthetic Organelle of the Amoeba Paulinella chromatophora. *Current Biology* **2017**,
987 *27*, 2763–2773, doi:10.1016/j.cub.2017.08.010.
988 102. Won, H.S.; Kang, S.J.; Lee, B.J. Action mechanism and structural requirements of the
989 antimicrobial peptides, gaegurins. *Biochimica et Biophysica Acta - Biomembranes* **2009**, *1788*,
990 1620–1629, doi:10.1016/j.bbamem.2008.10.021.
991 103. Conlon, J.M. Reflections on a systematic nomenclature for antimicrobial peptides from
992 the skins of frogs of the family Ranidae. *Peptides* **2008**, *29*, 1815–1819,
993 doi:10.1016/j.peptides.2008.05.029.
994 104. Haney, E.F.; Hunter, H.N.; Matsuzaki, K.; Vogel, H.J. Solution NMR studies of
995 amphibian antimicrobial peptides: linking structure to function? *Biochim. Biophys. Acta* **2009**,
996 *1788*, 1639–1655, doi:10.1016/j.bbamem.2009.01.002.
997

998

999

1000 ## Figure legends
1001

1002 **Figure 1. TPs cluster with certain types of HA-RAMPs.** (A) Contribution of the different groups
1003 of peptides, as described by 36 ACC terms, to the 2 clusters obtained by k-means (Chi^2 Pearson
1004 test, $p < 4.94 \cdot 10^{-324}$). The average silhouette coefficient is indicated above the graph. HA-
1005 RAMPs are depicted in blue in cluster 1 and in red in cluster 2. (B) Proportion of peptides among
1006 the 2 clusters for each group. Total number of peptides is indicated above bars. See figure panel
1007 for colour code. (C) Percentage of peptides from the HA-RAMP families described in the literature
1008 among classes I and II.

1009 **Figure 2. TPs and Class I HA-RAMPs display similar general features.** Distributions are
1010 represented by coloured box plots and individual values by coloured points; black diamond indicate
1011 mean values (A) Maximum hydrophobicity for a 9-residues window along the peptide. (B) Net
1012 charge of the peptide. (C) Number of amino acids that can formally adopt an amphiphilic α helical
1013 structure within the peptide (minimum of 9 residues). (D) Peptide length in amino acids. Numbers
1014 above distributions indicate the number of peptides represented (note that some peptides have no
1015 predicted amphiphilic helix). Stars indicate significant differences (Wilcoxon tests, p-value < 0.05)
1016 between that distribution and the distribution with the same colour as the star.
1017

1018 **Figure 3. TPs display amphiphilic properties.** Distributions are represented by coloured box
1019 plots as in Figure 2. (A) Number of amino acids that can formally adopt an amphiphilic α helical
1020 structure within the peptide. (B) Peptide length in amino acids. (C) Proportion of peptide predicted
1021 as amphiphilic (D) Net charge of the predicted helix. Numbers above distributions indicate the
1022 number of peptides represented (note that some peptides have no predicted amphipatic helix). Stars
1023 indicate significant differences (Wilcoxon tests, p-value < 0.05) between that distribution and the
1024 distribution with the same colour as the star.
1025

1026 **Figure 4. TPs and class I HA-RAMPs share similar physico-chemical properties.** PCA is
1027 performed on peptides described by 36 ACC terms. Peptide positions are plotted along the first
1028 (PC1) and second (PC2) principal component on the x and y axes respectively, with explained
1029 variance in parenthesis. Solid lines represent the convex areas containing the 50% most central
1030 peptides of each group. Groups are class I HA-RAMPs (blue) as defined in Figure 2, TPs (mTPs,
1031 orange triangle; cTPs, green triangle), SPs (eSPs, dark green cross; bSPs, indigo cross; tSPs, light
1032 green cross) and control peptides (globular AMP pink circle; random peptide yellow square). See

1033 Supplementary Figure 5A for the contribution of ACC terms PC1 and PC2 and Supplementary
1034 Figure 8 for PCA with class II HA-RAMPs.

1035 **Figure 5. AMPs function as TPs**. Constructs, schematically depicted at the top of the figure,
1036 assay the targeting ability of candidate peptides fused to the Venus-FLAG reporter, driven by the
1037 chimeric HSP70-RBCS promoter and the *RBCS2* 5'UTR (AR^P) and RBCS2 terminator ($R2^T$), and
1038 expressed bicistronically via the STOP-TAGCAT (*) sequence with the paromomycin resistance
1039 marker ($AphVIII^R$). Vertical lines indicate stop codons. Expression levels in *C. reinhardtii* are
1040 increased by the use of introns: RBCS2 intron 1 (i1) in the 5' UTR and RBCS2 intron 2 (i2) within
1041 the Venus coding sequence. Candidate HA-RAMPs, i.e. bacillocin 1580 (A), enterocin HF (B),
1042 sarcotoxin-1D (C), brevinin-2ISb (D) and magainin II (E) were fused to the RBCA cleavage site
1043 fragment encompassing residues -10 to +23 (RBCA-cs) and inserted upstream of Venus. The site
1044 of cleavage is indicated by a downward arrow. False-colour confocal images of representative cells
1045 show mitochondria as indicated by mitotracker fluorescence in cyan, the localisation of Venus in
1046 yellow and chlorophyll autofluorescence in magenta. Scale bars are 5μm. See Supplementary
1047 Figure 9 for a quantification of co-localisation, Supplementary Figure 10 for replicates, and Table
1048 S6 for a description of peptide sequences.

1049 **Figure 6. Biochemical confirmation of AMP targeting activity.** Mitochondrial, whole cell and
1050 chloroplast fractions (1 μg protein per well) isolated from Chlamydomonas strains in which Venus
1051 localisation is driven by bacillocin 1580 (A) or magainin II (B), each fused to the RBCA cleavage
1052 site, were immunolabelled with antibodies raised against against FLAG, an epitope tag carried C-
1053 terminally by the Venus reporter, and markers for different cellular compartments: Cytochrome
1054 Oxidase subunit IIb (COXIIb) and ATPsynthase subunit F1β for mitochondria (mt), Photosystem
1055 II Oxygen Evolving Enhancer 2 (OEE2) and Rubisco small subunit (RBCS) for chloroplasts (cp),
1056 α-Tubulin and nucleic-acid binding protein 1 (NAB1) for the cytosol (cyt) and lumenal binding
1057 protein (BiP) for the endoplasmic reticulum (ER). Isolated chloroplasts from the Bacillocin 1580
1058 strain (C) and isolated mitochondria from the Magainin II strain (D) were subjected to a proteinase
1059 assay, where aliquots were treated with either 150 μg ml^{-1} proteinase K and/or 1% Triton X-100, a
1060 membrane solubilising detergent. Aliquots were subsequently immuno-labelled with antibodies
1061 against FLAG, chloroplast ATP synthase subunit CF1 β and other organelle-markers described
1062 aside.

1063 **Figure 7. TPs exhibit antimicrobial activity.** *B. subtilis* was challenged with serial dilutions of
1064 synthetic peptides (See Table S7 for sequences): the *Rattus norvegicus* peptide hormone
1065 cholecystokinin-22, the *C. reinhardtii* tSP of lumenal 16.5 kDa protein, the HA-RAMP magainin
1066 II, *Neurospora crassa* mTP of ATP synthase F1β subunit and *C. reinhardtii* cTPs from RBCA and
1067 plastocyanin (PCY1) or mTPs from cytochrome c oxidase 12 kDa subunit (COX13) and Serine
1068 HydroxylMethyl Transferase 1 (SHMT1). Transparent wells illustrate absence of growth. Red
1069 arrows point to the minimal peptide inhibiting concentration.
1070

1071 ## Figures

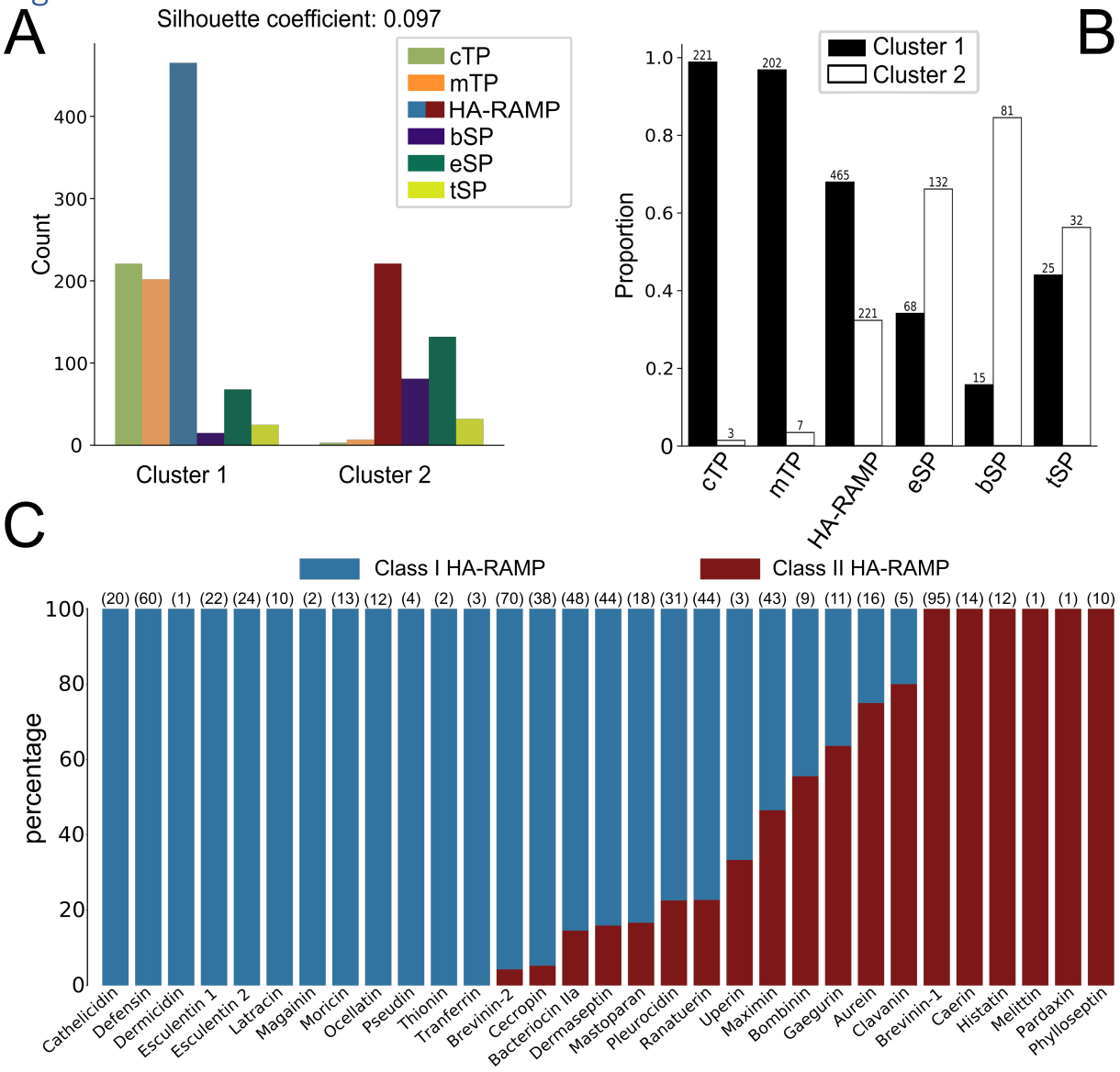

1072

Figure 1.

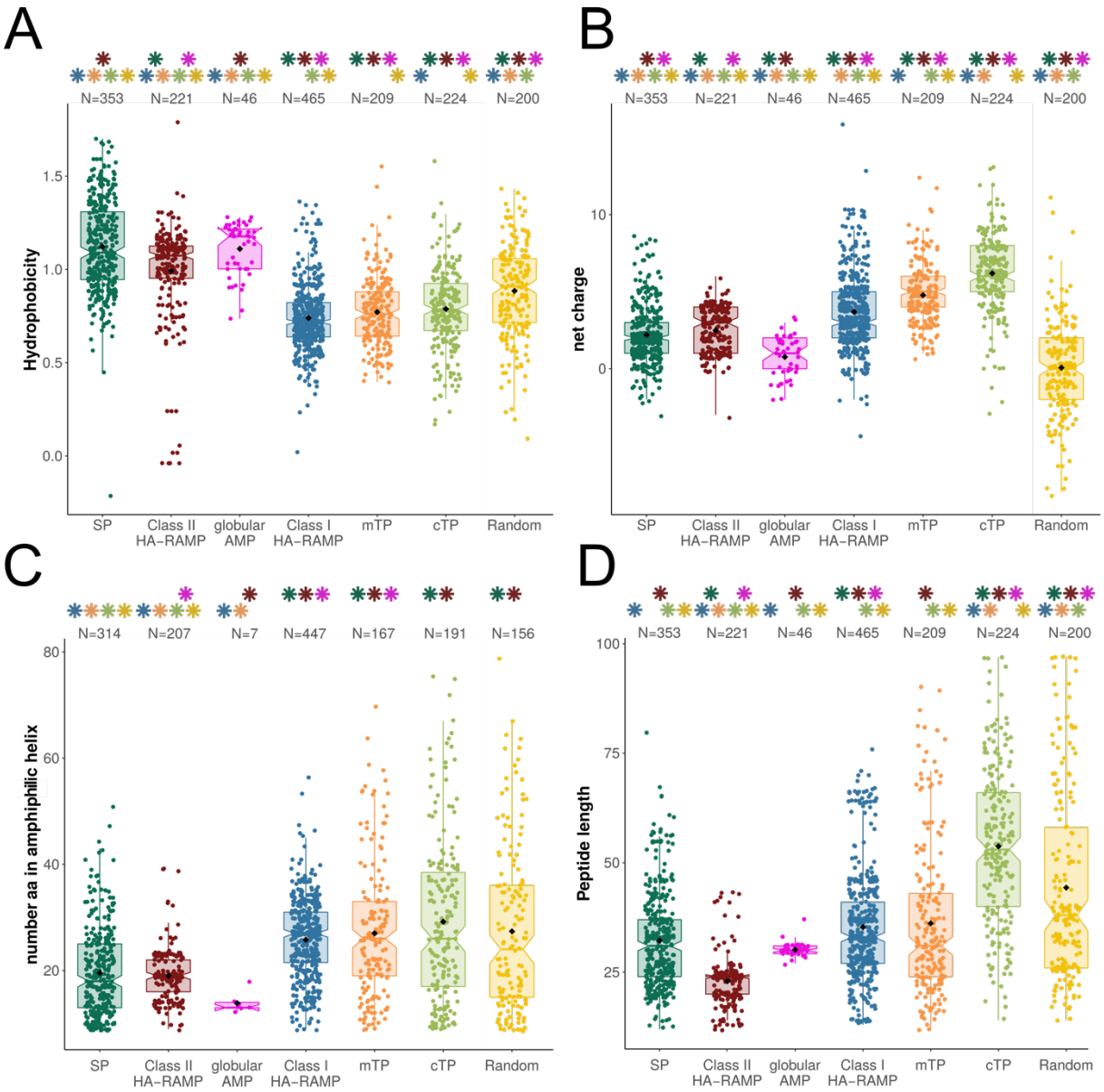

Figure 2.

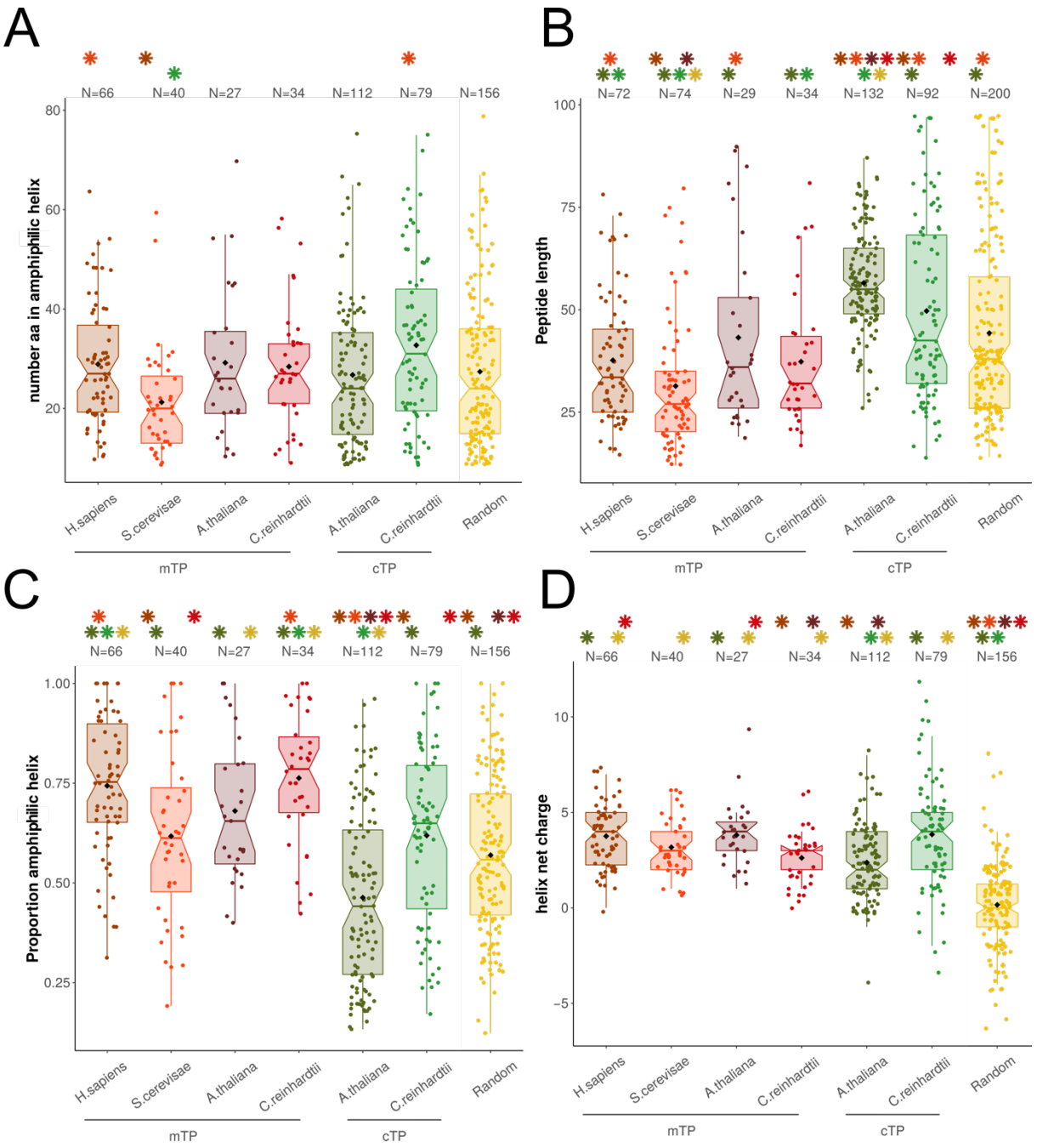
A
B
C
D
number aa in amphiphilic helix
Peptide length
Proportion amphiphilic helix
helix net charge
N=66
N=40
N=27
N=34
N=112
N=79
N=156
N=72
N=74
N=29
N=132
N=92
N=200
H.sapiens
S.cerevisae
A.thaliana
C.reinhardtii
A.thaliana
C.reinhardtii
Random
mTP
cTP

Figure 3.

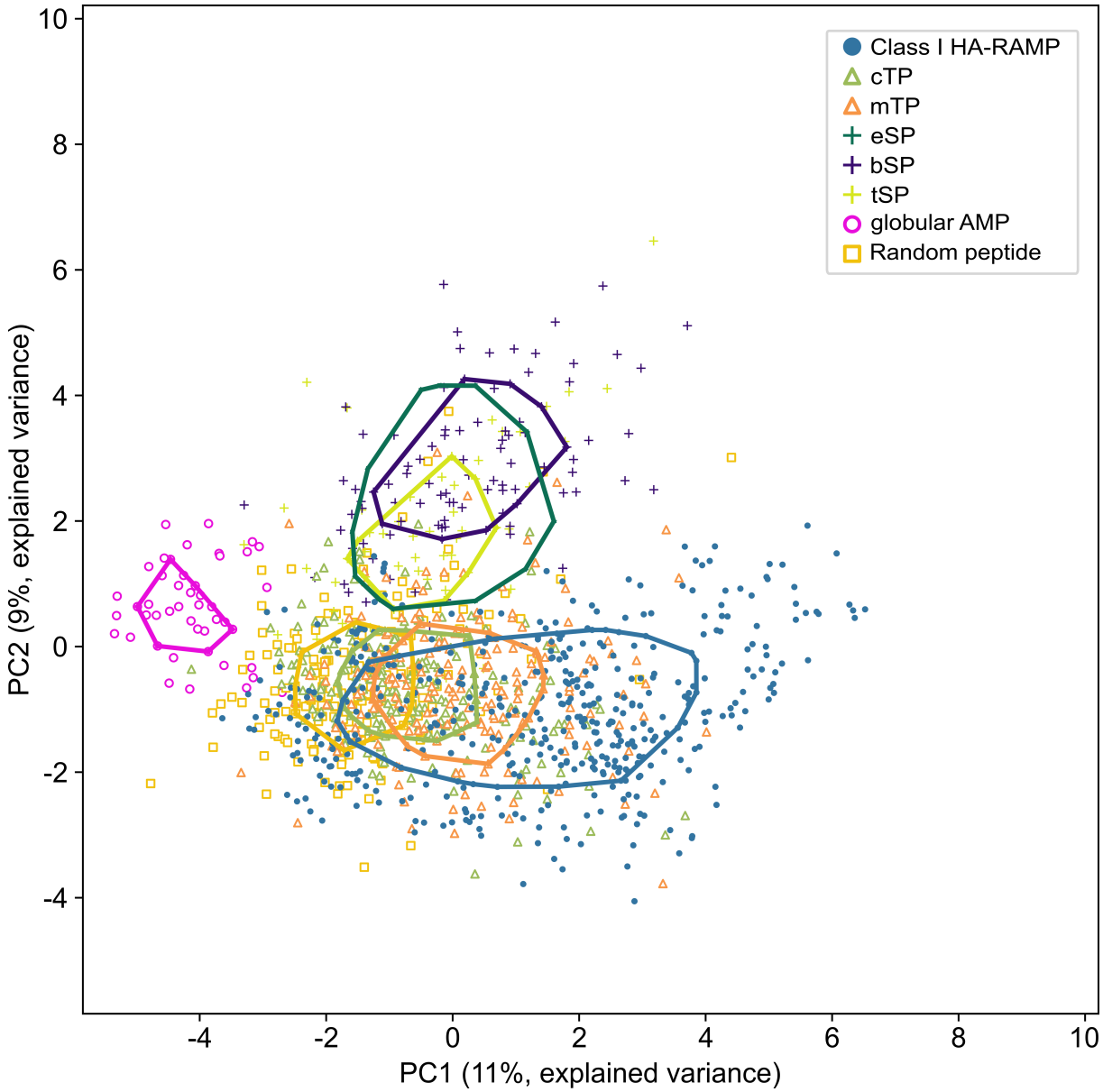
Class I HA-RAMP
cTP
mTP
eSP
bSP
tSP
globular AMP
Random peptide
PC2 (9%, explained variance)
PC1 (11%, explained variance)
10
8
6
4
2
0
-2
-4
-4
-2
0
2
4
6
8
10

Figure 4.

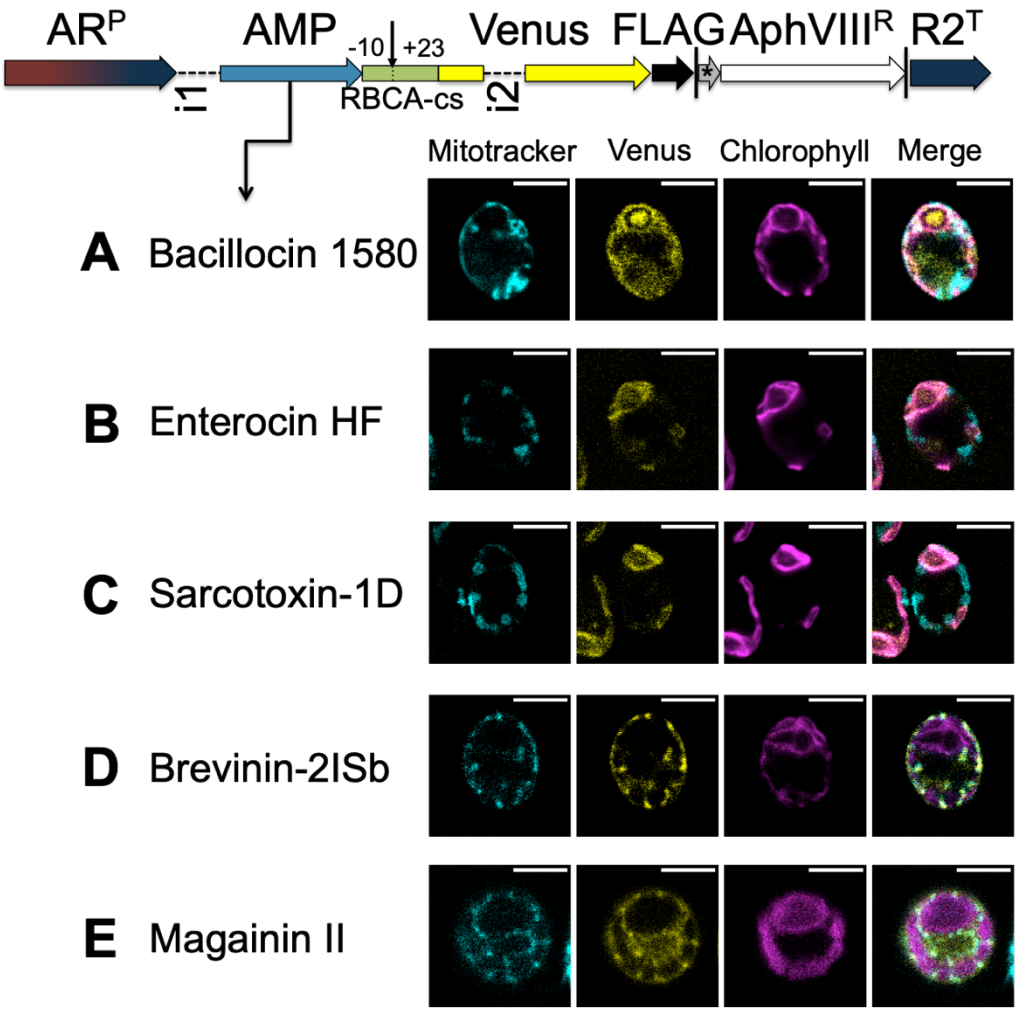
ARP
AMP
-10
+23
Venus
FLAG
AphVIIIR
R2T
i1
RBCA-cs
i2
Mitotracker
Venus
Chlorophyll
Merge
A Bacillocin 1580
B Enterocin HF
C Sarcotoxin-1D
D Brevinin-2ISb
E Magainin II

Figure 5.

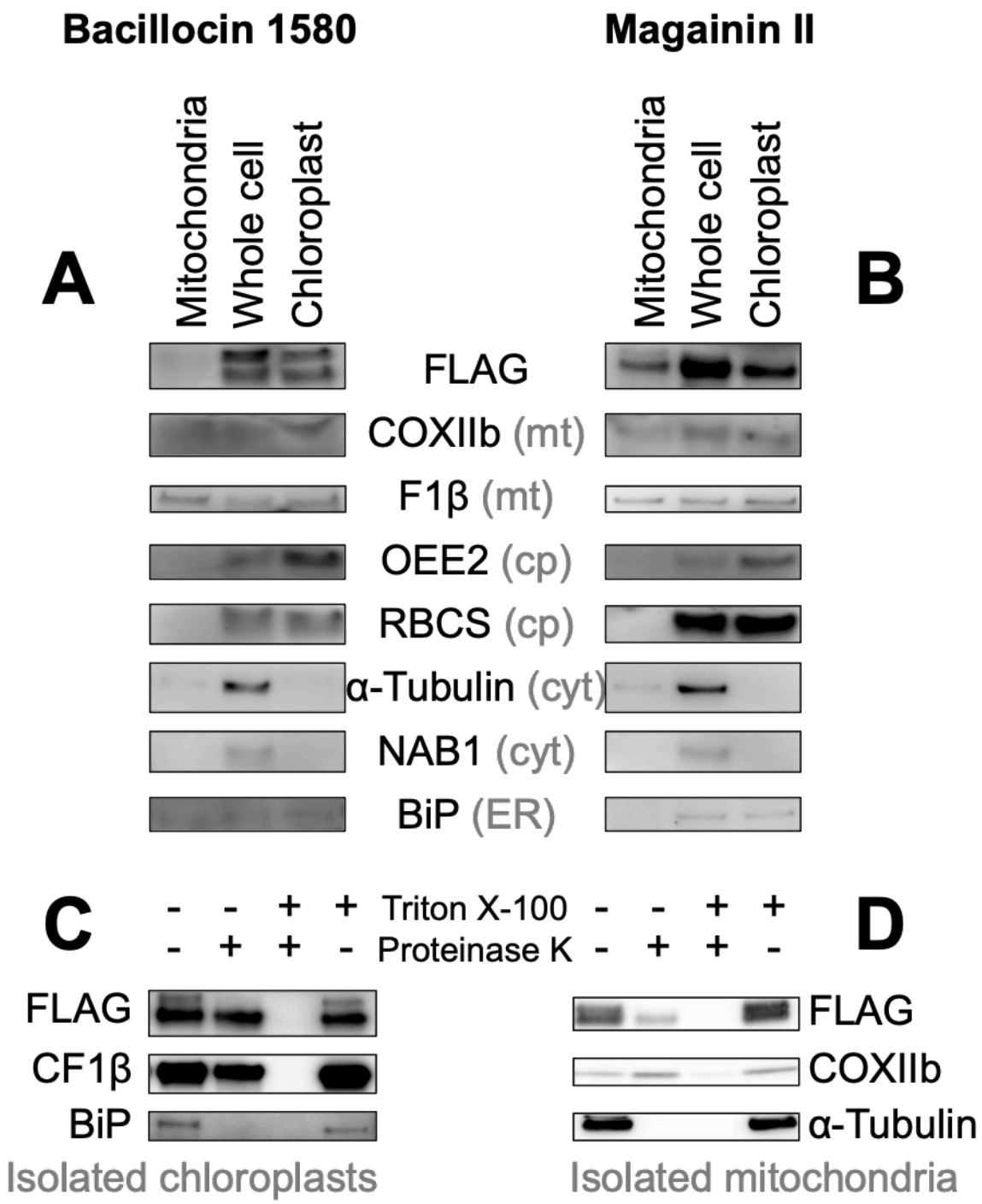
Bacillocin 1580
Magainin II
A
B
Mitochondria
Whole cell
Chloroplast
FLAG
COXIIb (mt)
F1β (mt)
OEE2 (cp)
RBCS (cp)
α-Tubulin (cyt)
NAB1 (cyt)
BiP (ER)
C
D
Triton X-100
Proteinase K
FLAG
CF1β
BiP
COXIIb
α-Tubulin
Isolated chloroplasts
Isolated mitochondria

Figure 6.

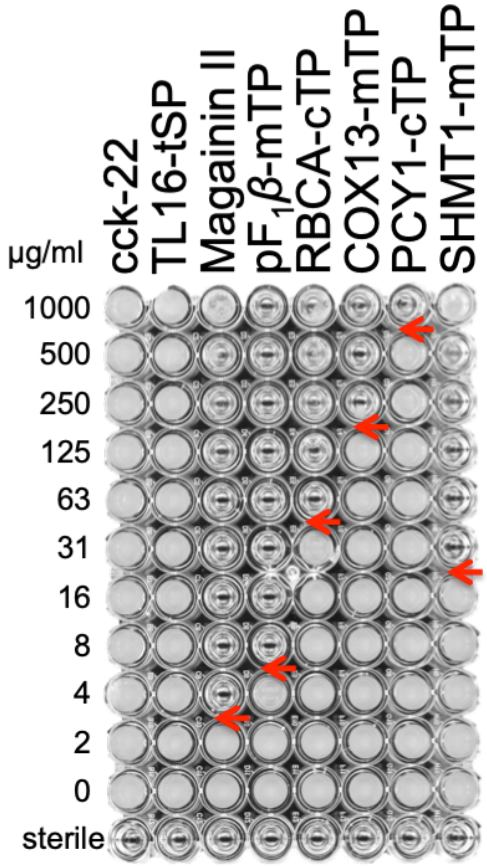
cck-22
TL16-tSP
Magainin II
pF1β-mTP
RBCA-cTP
COX13-mTP
PCY1-cTP
SHMT1-mTP
µg/ml
1000
500
250
125
63
31
16
8
4
2
0
sterile

Figure 7.